Theophylline acetaldehyde as the initial product in doxophylline metabolism in human liver

Xiaohua Zhao[1,2], Hong Ma[3,4], Qiusha Pan[1,2], Haiyi Wang[1,2], Xingkai Qian[1,2], Peifang Song[1,2], Liwei Zou[1,2], Mingqing Mao[5], Shuyue Xia[5], Guangbo Ge[1,2], Ling Yang[1,2*]

[1]Institute of Interdisciplinary Integrative Medicine Research, Shanghai University of Traditional Chinese Medicine, Shanghai 201203, China

[2]Center for Systems Pharmacokinetics, Shanghai University of Traditional Chinese Medicine, Shanghai 201203, China

[3]College of Basic Medical Sciences, Dalian Medical University, Liaoning 116044, China

[4]Shanghai Research Institute of Acupuncture and Meridian, Shanghai 200030, China

[5]Respiratory Medicine Department, Central Hospital Affiliated to Shenyang Medical College, Liaoning 110034, China

Running Title: Identification of the initial metabolite of doxophylline

Corresponding author and contact information:

Ling YANG

Corresponding author at: Institute of Interdisciplinary Integrative Medicine Research, and Center for Systems Pharmacokinetics, Shanghai University of Traditional Chinese Medicine, Shanghai 201203, China

Mailing address: No.1200, Cailun Road Shanghai 201203, China

Phone: +86 21 51323185.

Email address: yling@shutcm.edu.cn (L Yang)

Text Page: 25

Number of tables: 0

Number of figures: 6

Number of references: 27

Number of words:

Abstract: 202

Introduction: 837

Discussion: 1344

Abbreviations: 1-ABT, 1-aminobenzotriazole; AP, aminophylline; AUC, area under the plasma concentration-time curve; Brij 58, polyethylene glycol hexadecyl ether; CA, caffeine; COPD, chronic obstructive pulmonary disease; CyLM, monkey liver microsomes; CYP, cytochrome P450; DOXO, doxophylline; ETO, etophylline; HET, 2'-hydroxyethyl ester

theophylline acetic acid; HLM, human liver microsomes; HLS9, human liver S9; HRMS, high resolution mass spectrometry; i.v., intravenous; MLM, mouse liver microsomes; NMR, nuclear magnetic resonance, PX, paraxanthine; RaLM, rabbit liver microsomes; RLM, rat liver microsomes; SER, smooth endoplasmic reticulum (microsomes); TAA, theophylline-7-acetic acid; TA, theophylline-7-acetaldehyde; TB, theobromine; TP, theophylline; UDPGA, uridine 5'diphosphoglucuronic acid; VD, apparent volume of distribution.

Abstract

Doxophylline (DOXO) and theophylline are widely used as bronchodilators for treating asthma and chronic obstructive pulmonary disease, and DOXO has a better safety profile than theophylline. How DOXO metabolism and disposition affect its anti-asthmatic efficacy and safety remains to be explored. In this study, the metabolites of DOXO were characterized. A total of nine metabolites of DOXO were identified *in vitro* using liver microsomes from human and four other animal species. Among them, six metabolites were reported for the first time. The top three metabolites were theophylline acetaldehyde (M1), theophylline-7-acetic acid (M2) and etophylline (M4). A comparative analysis of DOXO metabolism in human using liver microsomes, S9 fraction, and plasma samples demonstrated that: (1) The metabolism of DOXO began with a CYP-mediated, rate-limiting step at the C ring and produced M1, the most abundant metabolite in human liver microsomes. However, in human plasma, the M1 production was rather low. (2) M1 was further converted to M2 and M4, the end products of DOXO metabolism *in vivo*, by non-CYP dismutase in the cytosol. This dismutation process also relied on the ratio of $NADP^+$/NADPH in the cell. These findings for the first time elucidated the metabolic sites and routes of DOXO metabolism in human.

Significance Statement:

We systematically characterized doxophylline metabolism using *in vitro* and *in vivo* assays. Our findings evolved the understandings of metabolic sites and pathways for methylxanthine derivatives with the aldehyde functional group.

Introduction

Doxophylline (DOXO), theophylline (TP), aminophylline (AP) (Spina and Page, 2017), etophylline (ETO) (Sharma and Sharma, 1979) and caffeine (CA) are methylxanthine derivatives, and the first four compounds have been approved for use in clinical practice. Among them, TP and DOXO are clinically more effective and widely used in the treatment of asthma and chronic obstructive pulmonary disease (COPD). A recent meta-analysis of 696 asthma patients shows that DOXO has slightly better efficacy and a much better profile of safety than TP (Rogliani et al., 2019), hence has a broader therapeutic window in treating asthma. DOXO also shows fewer side effects on cardiac function (Dini and Cogo, 2001), sleep rhythm (Sacco et al., 1995), gastric secretions (Lazzaroni et al., 1990) and central nervous system (Cravanzola et al., 1989), and exhibits lower risks of drug-drug interaction (Mennini et al., 2017). In February 2014, the US FDA granted an orphan drug designation to DOXO for treating bronchiectasis (https://www.accessdata.fda.gov/scripts/opdlisting/oopd/detailedIndex.cfm?cfgridkey=399413). Efforts have been made to understand the mechanism underlying the superior safety profile of DOXO. Studies show that DOXO exhibits rather weak effects on the well-characterized *in vivo* targets of TP, such as phosphodiesterase and adenosine receptors (van Mastbergen et al., 2012). These evidence are insufficient to justify the equivalent efficacy and better safety of DOXO in clinical usage. Therefore, the molecular mechanism of DOXO still remains to be investigated.

The metabolic stability of a compound is determined by its structure. TP, CA and DOXO share identical parental skeleton, and differ only in the N-7 substituent groups. We assigned A, B and C rings to the structures of DOXO to accurately describe the metabolic sites and derivative functional groups (Fig. 1).

TP lacks a substituent group at the N-7 position and has the lowest *in vivo* metabolic rate among the three drugs. The primary metabolic pathways of TP are demethylation at the N-1 and N-3 positions (Fig. 1). The area under the plasma concentration-time curve (AUC) of TP accounts for about 91% of the total AUC in human plasma after oral TP administration (Rodopoulos and Norman, 1997). Therefore, the widely observed fluctuation of TP concentration in the blood among different individuals (Bertil, 2010) is mainly attributed to other factors, rather than the instable structure of the compound. One possible cause is TP has a large variation in apparent volume of distribution (VD) (Tanikawa et al., 1999) and the strong tissue binding activity (Shum and Jusko, 1987). Once binding competition occurs (Troger and Meyer, 1995), plasma concentration of TP could be highly volatile, leading to side effects such as cardiac- and neuro-toxicity (Minton and Henry, 1996).

CA has a methyl group at the N-7 position and the overall demethylation activity increases. In human, CA metabolized to paraxanthine (PX, 84%), theobromine (TB, 12%) and TP (4%). These three metabolites could be further demethylated (Nehlig, 2018). The AUC of parent drug CA in human plasma accounts for 56% of the total AUC (Martinez-Lopez et al., 2014). It's worth noting that CA metabolite profiles exhibit significant variation between individuals. The demethylation of CA and TP is primarily catalyzed by CYP1A (Fort et al., 1996). Several studies show distinct differences in the metabolic capacity of CYP1A among individuals (Dai et al., 2017; Dai et al., 2015). It's been recently demonstrated that CYP2E1 also participates in CA metabolism, which would further contribute to the metabolic variation of CA (Nehlig, 2018). Therefore, the individual variation of CA concentration in human blood arises from both the structural instability and the variation of metabolic enzyme activity.

DOXO has a 1,3-dioxolane ring (cyclic acetal) at the N-7 position. Previous studies show that DOXO is relatively stable in rat liver microsomes (RLM) as 95% of the parent compound has been recovered. The metabolites detected in RLM are TP and 2'-hydroxyethyl ester

theophylline acetic acid (HET) (Grosa et al., 1986). However, these two products are not present in human serum. Clinical pharmacology studies of oral and i.v. administered DOXO show distinct individual variation of ADME profiles for DOXO (Shukla et al., 2009). The biological instability of DOXO *in vivo* is characterized by quick elimination and short half-life. The only metabolite detected in the human blood is the inactivated etophylline (ETO). Therefore, DOXO has been proposed as the active compound rather than the pro-drug responsible for its clinical efficacy and safety (Matera et al., 2017).

Our recent study also demonstrated that DOXO was instable in human. We identified theophylline-7-acetic acid (TAA) to be a new product of DOXO metabolism *in vivo* in addition to ETO, and the AUC of intact DOXO in plasma after i.v. drip was only 27% (Fang et al., 2019). Taken together, the published studies on DOXO metabolism focus on the pharmacokinetics of prototype compound, whereas *in vitro* evidence on biochemical stability and drug metabolism of DOXO are limited. In this study, we performed a systematic investigation and comparative analysis on DOXO metabolism using human liver microsomes, human liver S9 and human blood serum. We identified and characterized the metabolites of DOXO and illustrated the interconversion relationships *in vitro* and *in vivo*.

Materials and Methods

Chemicals and Reagents. DOXO (99.7%), TP (99.5%) and ETO (99.7%) were purchased from Dalian Meilunbio. Co., Ltd (Dalian, China). Theophylline-7-acetaldehyde (TA 91.4%) was bought from Beijing Comparison Pharmaceutical Tech. Co., Ltd (Beijing, China). TAA (99.7%) was from Aladdin Industrial Corporation (Shanghai, China). D-glucose 6-phosphate (G6P), glucose-6-phosphate dehydrogenase (G6PDH), β-$NADP^+$, NADPH, UDPGA trisodium salt, Brij 58 and 1-aminobenzotriazole (1-ABT) were obtained from Sigma-Aldrich (St. Louis, MO). HET (92.7%) was synthesized by Professor Guoliang Chen at Shenyang Pharmaceutical University (Shenyang, China). All other reagents were either LC grade or the highest grade commercially available.

Enzyme Sources. Pooled liver microsomes from human (HLM), mouse (MLM), rabbit (RaLM), rat (RLM), monkey (CyLM) and pooled human liver S9 (HLS9) were purchased from Research Institute for Liver Diseases (Shanghai) Co. Ltd (Shanghai, China) and stored at -80℃.

In Vitro Incubation Reaction. The total volume of each incubation was 200 μL and organic solvent did not exceed 2 μL.

For phase I metabolism, incubation was performed in PBS buffer (0.1 M, pH=7.4). The incubation system contained liver microsomes/HLS9 (0.5 mg/mL), DOXO/TA/TAA/ETO/HTE (100 μM) and NADPH-regenerating system including G6PDH (1 U/mL), $MgCl_2$ (5 mM), G6P (10 mM) and β-$NADP^+$ (1 mM). After pre-incubation for 5 minutes, the reaction was initiated by adding β-$NADP^+$. The mixtures incubated 60 minutes at 37℃ on a thermo-shaker. To inhibit the CYP activity in phase I metabolism, 1-ABT (500 μM) was pre-incubated with HLM/HLS9 and NADPH-generating system for 20 minutes at 37℃, then DOXO was added.

For phase II metabolism, the incubation system contained 50 mM Tris-HCl (pH 7.4), HLM (0.5 mg/mL), DOXO/TAA/ETO (100 μM), UDPGA (2 mM), $MgCl_2$ (5 mM) and Brij 58 (0.1 mg/mg protein).

For kinetics analysis, the incubation system contained PBS (0.1 M, pH 7.4), HLS9 (0.1 mg/mL), TA (1~500 μM) and β-$NADP^+$ / freshly prepared NADPH (1 mM). The reaction was initiated by adding HLS9 and the incubation time was 6 minutes.

For chemical stability test, 100 μM DOXO was incubated in 0.2% formic acid at 37℃ for 60 minutes.

All these reactions were terminated by adding 100 μL ice-cold acetonitrile, and then centrifuged at 20,000g for 20 minutes at 4℃. Incubation systems without liver microsomes/HLS9, co-factor or substrate were used as controls.

Ethics Approval and Human Subjects. This research was approved by the Independent Ethics Committee in 2018, January (Approval #: 2018 [00021]). Human subjects enrolled in this project were informed the purpose, procedure and risk of the study. Three volunteers were female, Asian, and aged 25, 25, 26. Physical exams were performed before the enrollment, and no pathological conditions were found.

Protocol for drug administration and blood sampling. Under fasting conditions, 100 mg DOXO was administered as single dose by i.v. drip for 30 minutes. Blood samples were collected from the contralateral antecubital vein at pre-dose, and at 0.25, 0.5, 0.75, 1, 1.25, 1.5, 2, 2.5, 4.5, 6.5, 8.5, 10.5, 12.5, 24.5 h after the i.v. administration started. Plasma was immediately separated from the blood by centrifugation at 4450 g for 10 minutes at 4℃ and stored at -20℃.

Sample Preparation for MS analysis. For *in vitro* samples, 3 μL of the supernatant was used for LC-Triple TOF analysis. The supernatant was diluted with 0.2% formic acid (v: v=1:2), and 1 μL was used for LC-MS/MS analysis. For plasma preparation, 25 μL sample was

deproteinized with 75 μL acetonitrile. The mixture was diluted with 100 μL water containing 0.2% formic acid. After centrifugation for 20 minutes at 20,000 g, 5 μL of the supernatant was used for LC-Triple TOF and 2 μL for LC-MS/MS.

LC-Triple TOF Analyses. Metabolite identification was performed on a 5600+ TripleTOF® quadrupole-time of flight mass spectrometer equipped with a DuoSpray source (Sciex). The mass spectrometer was coupled with an ExionLC system. Chromatographic separation was performed on an Acquity UPLC® BEH C18 column (3.0×100 mm i.d., 1.7 μm; Waters). A 15-minute gradient with water containing 0.2% formic acid (A) and acetonitrile containing 0.2% formic acid (B) was used at a flow rate of 0.3 mL/minute. Injection volume was 3 μL for all samples. Autosampler and column oven temperatures were maintained at 4°Cand 50°C, respectively. Ionization was operated using an electrospray ionization (ESI) source. Data were collected in the positive ion mode with Analyst TF software version 1.7.1 (Sciex). The mass spectrometer was conducted in full-scan TOF-MS (*m/z* 100-1000) combined with information-dependent acquisition (IDA) MS/MS modes, the collision energy was set as 15 ± 10 eV. Both ion source gas 1 and 2 were set to 50 psi. Curtain gas was set to 35 psi. The ionspray voltage floating was 5500V and temperature was 550°C.

LC-MS/MS Analysis. Metabolite detection was performed on a 4500 QTRAP® mass spectrometer (triple quadrupole-linear ion trap) equipped with a TurboV ion source (Sciex). The mass spectrometer was coupled with an LC-20ADXR HPLC system (Shimadzu). DOXO and its metabolites were separated on a UPLC® BEH C18 (2.1×50 mm i.d., 1.7 μm; Waters) analytical column. The mobile phase was flowing at 0.35 mL/minute and composed of water containing 0.2% formic acid (A) and acetonitrile (B). The gradient elution mode was applied. Data was acquired and processed with the Analyst software version 1.6.3 (Sciex). Detection of the ions were operated in the positive multiple-reaction monitoring (MRM) mode. The ion transitions for analytes were monitored and summarized in Stable. 1. Ion source gas 1 and 2

were set to 55 and 60 psi, respectively. The temperature and ionspray voltage floating were 550℃ and 5500 V, respectively. Curtain gas was at 40 psi. Collision gas was set at medium. The collision energy and declustering potential for all compounds were 27 and 65 eV. The MRM chromatograms for metabolic products in HLM, HLS9, human plasma and blank control under the above conditions were shown in SFig. 1.

Results

LC-Triple TOF Analyses of DOXO and metabolites. To identify the unknown metabolites, we first used LC-Triple TOF to investigate the chromatographic behavior, characteristic ions and mass fragmentation pattern of DOXO. In the positive ion mode, DOXO was eluted at 6.7 minutes (SFig. 2A) with a protonated molecular ion at *m/z* 267.1085. The MS^2 spectrum of DOXO exhibited major fragment ions at *m/z* 223.0814, 210.0867, 181.0712, 166.0602, 138.0654, and 124.0494 (SFig. 2B). The tentative MS^2 fragmentation pattern and identification of fragment ions were displayed in SFig. 2C. The fragment ion at *m/z* 223.0814 was formed via the cleavage of two C-O bonds on the 1,3-dioxolane ring. The ion at *m/z* 210.0867 was generated by the loss of tertiary amides from the A ring. The ions at *m/z* 181.0712 and 124.0494 were the structurally diagnostic ions of TP. The ion at *m/z* 138.0654 was produced by the loss of 1,3-dioxolane ring from the fragment ion at *m/z* 210.0867. The *m/z* 166.0602 ion was formed by the loss of tertiary amides from the ion at *m/z* 223.0814.

Then we characterized the metabolites of DOXO in the HLM incubation system. A total of nine metabolites were detected, and six of them, M1, M2, M6, M7, M8, M9, were reported for the first time. The preliminary structures of these metabolites were examined. Among them, M1 was the most abundant metabolite. Six of these nine metabolites were derived from the metabolism of the C ring, including M1 (TA), M2 (TAA), M3 (TP), M4 (ETO), M5 (HET), and M9 (DOXO dehydrogenation product) (SFig. 3), and their structures were confirmed by standard references. The other three metabolites, M6, M7 and M8, were derived from metabolism on the A and B rings and were analyzed by ion fragment pattern to predict the structures and metabolic sites (SFig. 3). No glucuronide conjugate was detected in Phase II metabolism in HLM (SFig. 8).

M1 was eluted at 5.1 minutes, and its protonated molecular ion was at *m/z* 223.0828 with elemental composition $C_9H_{10}N_4O_3$. The ion at *m/z* 241.0935 was the hydrated protonated ion

of M1. The ions at *m/z* 124.0499 and 181.0720 suggested that the A and B rings remained unchanged, and the ions at *m/z* 138.0660 and 195.0875 implied that the B ring was linked with a methyl group. Based on these observations, we hypothesized M1 to be TA. It was verified by a comparing of the chromatography and mass spectra between M1 and the reference standard of TA. The MS^2 spectrum and the speculated molecular structure of M1 are shown in SFig. 3A.

M2 was eluted at 4.65 minutes and the elemental composition was $C_9H_{10}N_4O_4$. Compared to DOXO, M2 was short of a C_2H_4. The precursor ion at *m/z* 239.0772 and its dehydration ion at *m/z* 221.0653 indicated that there was a hydroxyl group in M2. The ions at *m/z* 124.0495, 138.0640, and 181.0708 suggested the presence of unmodified A and B rings. Thus, the dealkylation occurred on the 1,3-dioxolane ring and M2 was identified to be TAA (SFig. 3B). It was further confirmed by a comparison to the TAA reference standard.

M3 was eluted at 4.67 minutes and exhibited a molecular ion peak at *m/z* 181.0714. The elemental composition of metabolite M3 was $C_7H_8N_4O_2$, identical to that of TP. The characteristic fragment ion was at *m/z* 124.0502. By comparing the chromatographic and MS behavior between M3 and the reference standard, we confirmed M3 to be TP (SFig. 3C).

M4 was eluted at 5.24 minutes and showed a protonated molecular ion at *m/z* 225.0969 with elemental composition of $C_9H_{12}N_4O_3$, which suggested the loss of a C_2H_2O from the parent drug DOXO. The dehydration ion at *m/z* 207.0872 indicated the presence of a hydroxyl group in M4. The ions at *m/z* 124.0490 and 181.0713 implied that the metabolic reactions occurred on the 1,3-dioxolane ring. Therefore, M4 was proposed to be ETO, and it was confirmed by a comparison with the reference standard (SFig. 3D).

M5 was eluted at 5.58 minutes with protonated molecular ion at *m/z* 283.1033. The elemental composition of M5 was $C_{11}H_{14}N_4O_5$, suggesting that it was monohydroxylated product of DOXO. M5 shared the same fragment ions with M2 at *m/z* 124.0502, 181.0711, 193.0712,

221.0656 and 239.0769 (SFig. 3E), indicating that the two compounds had similar chemical structure segment. The ion at *m/z* 265.0192 was a dehydrated ion. These observations collectively suggested that an oxygen atom was introduced into the 1,3-dioxolane ring, followed by a ring-opening reaction and dehydrogenation. In addition, a previous study showed that HET was the major metabolite of DOXO in RLM (Grosa et al., 1986). Taken together, we proposed M5 to be HET and it was confirmed by comparison with the chemically synthesized reference standard.

M9 showed a $[M+H]^+$ ion at *m/z* 265.0923 with the elemental composition of $C_{11}H_{12}N_4O_4$. It was eluted at 6.36 minutes as a dehydrogenation product of DOXO. The presence of fragment ion at *m/z* 181.0710 indicated that the structure of the A and B rings remained intact and the dehydrogenation reaction occurred on the C ring (SFig. 3F).

M6 was eluted at 5.84 minutes with the same elemental composition as M5 ($C_{11}H_{14}N_4O_5$). Unlike M5, the MS/MS spectrum of M6 had the fragment ion at *m/z* 197.0662 rather than 181.0711 (SFig. 3G), suggesting that the oxygen was introduced to the A or B ring via a hydroxylation step. Considering the structural characteristics of the A and B rings and the metabolic sites of TP (Rodopoulos and Norman, 1997), this hydroxylation might occur at the C-8 position. This was also supported by the fact that no dehydration peak was found in M6. Of note, the peak area of M6 was less than 5% of the peak area of M5.

M7 and M8 had the same element composition of $C_{10}H_{12}N_4O_4$ and were eluted at 5.18 and 5.72 minutes, respectively. They possessed the same protonated molecular ions at *m/z* 253.092, which were 14 Da lower than DOXO, indicating that M7 and M8 were demethylated products of DOXO (SFig. 3H). The presence of the ion at *m/z* 167.0558 but not 181.0712 suggested that demethylation occurred at the N-1 or N-3 positions of the A ring. However, it was difficult to determine which demethylation product was dominant. In addition, the peak area of M7 was less than 5% of the peak area of M8.

The details for each metabolite, including retention time, accurate mass, molecular formula and fragmented ions were shown in Stable. 2. Reference standards of DOXO and the major metabolites, M1, M2, M4 and M5, were examined by HPLC, and the purity was quantified by peak area normalization method. The HPLC conditions and the chromatogram results were shown in STable. 3 and SFig. 4. The structures of these reference standards were characterized by high resolution mass spectrometry (HRMS) and nuclear magnetic resonance (NMR). The MS^2 spectra and NMR data were shown in SFig. 5-7.

Chemical stability of DOXO. We examined the chemical stability of DOXO and found that less than 0.1% DOXO was destroyed after a 60-minute incubation at 37℃ in 0.2% formic acid, and little M1 formation was detected under this condition. Thus, DOXO was chemically stable. The biochemical stability of DOXO was tested in following experiments.

Metabolism of DOXO in liver microsomes. To better understand the mechanism of *in vitro* DOXO metabolism, we compared the metabolite profiles in liver microsomes among five different species. The nine metabolites identified in HLM were also present in liver microsomes of mouse, rabbit, rat and monkey, and no additional novel metabolites were detected.

The metabolic rates of DOXO in different species was determined by LC-MS/MS. The formation of the four major metabolites, M1, M2, M4, and M5, were quantified. Due to the incomplete structure information and lack of reference standard compounds, the trace metabolites M8 and M9 were semi-quantitatively analyzed based on the calibration curve of M4. The typical calibration curves were shown in STable.4. The abundance of M3, M6, and M7 was extremely low in HLM, thus no further quantitative measurement was conducted. The metabolic rate was calculated based on the production of metabolites per milligram of protein per minute within a 2-hour incubation. The total rate of six metabolites for CyLM, RLM, RaLM, MLM and HLM was 888, 635, 555, 313, and 222 pmol, respectively (Fig. 2).

Among the five species, the total metabolic conversion rate of DOXO was the lowest in HLM, and the highest in CyLM. Based on the characteristic metabolite profile of each species, defined by the relative abundance of individual metabolite, the liver microsomal metabolism of the five species could be classified into two categories (Fig. 2): Type I was featured by one predominant metabolite M1, including HLM (87% M1) and RLM (88% M1). The only difference between HLM and RLM was that the amount of M5 in RLM was significantly higher than that in HLM. Type II was defined by the presence of two major metabolites, M1 and M4, including MLM (64% M1, 26% M4), CyLM (28% M1, 57% M4) and RaLM (31% M1, 62% M4). Of note, M1 was dominant in MLM, whereas M4 was dominant in CyLM and RaLM. What's in common between Type I and Type II metabolism was that, all the major metabolites were mainly derived from the metabolism of the C ring, rather than the A or B ring.

Metabolism of DOXO in human plasma. Three healthy volunteers were i.v. dripped with 100 mg DOXO for 30 minutes, and the plasma samples were collected and analyzed by LC-MS/MS. Four metabolites, M1, M2, M4 and M5, were quantitatively measured, whereas M8 and M9 were subjected to semi-quantitative examination. The results showed that M2 and M4 were the most abundant metabolites in plasma. The major *in vitro* product M1 in HLM was present at rather low abundance in plasma. M5, M8 and M9 were also present at trace amount. The plasma concentration-time curve for each metabolite was shown in Fig. 3.

Then we compared the concentration-time curves between DOXO and its key metabolites M1, M2, and M4 (Fig. 3). The parent drug DOXO was quickly eliminated after i.v. drip, and the elimination rate was about 50 L/h. The Tmax for M1 and M2 was at 0.5h and 0.75h in all three volunteers; and the Tmax for M4 was at 1, 1.5 and 2h, respectively, in the three volunteers. The sequence of the peak times for these three major metabolites indicated that M1 and M2 might be the initial or intermediate products in DOXO metabolism.

Identification of initial product in DOXO metabolism. To investigate the differences between *in vitro* and *in vivo* DOXO metabolism, we used DOXO, M1, M2, M4 or M5 as individual substrate (100 μM/each) and measured the formation of other compounds in HLM and HLS9 (Fig. 4).

When DOXO was used as substrate (Fig. 4A), the total percentage of M1, M2 and M4 in final products was about 98% in both HLM and HLS9, whereas the total amount of M5, M8 and M9 did not exceed 2%. In HLM, M1 accounted for 87% of the total metabolic products, while in HLS9, the ratio of M1 dropped to 26%. On the contrast, M2 and M4 together accounted for 11% of the total metabolites in HLM, and this ratio increased to 72% in HLS9, which was closely aligned with the *in vivo* data. These results indicated that the enzymes responsible for M2 and M4 formation were more likely to be in cytosol. Furthermore, when a broad-spectrum CYP inhibitor (1-ABT) was added to the HLM and HLS9 incubation systems, the production of M1, M2 and M4 was significantly reduced in both settings, suggesting that the formation of M2 and M4 was still liver microsomal system dependent. Based on these results, we proposed that, DOXO was metabolized to M1 by CYP enzymes, and M1 was further metabolized to M2 and M4 in cytosol. 1-ABT inhibited CYP activity to prevent the M1 formation, hence indirectly reducing the formation of M2 and M4.

To validate this speculation, we used standard references of M1, M2, M4, M5, the key metabolites produced in HLM, as substrates to investigate the continuous metabolism in HLS9.

When M1 was used as the substrate (Fig. 4B), only M2 and M4 were detected in both HLM and HLS9, confirming that M2 and M4 were products of M1 metabolism. Of note, similar amounts of M2 (derived from M1 oxidation) and M4 (derived from M1 reduction) were produced. The total amount of M2 and M4 in HLS9 was about 8-fold of that in HLM, further demonstrating that the cytosol enzymes were required for the M1 → M2 + M4 conversion. While 1-ABT had little impact on the production of M4, it partially inhibited the metabolism

of M2, and exerted a non-specific inhibitory effect on M1 oxidation. Taken together, these results strongly suggested that DOXO can hardly be directly converted to M2 or M4 without being firstly converted to M1, and that the DOXO to M1 conversion was the rate-limiting step at the beginning of the metabolic reaction chain.

When M2 or M5 was used as substrate, no above known metabolites or DOXO were detected in HLM or HLS9. When using M4 as the substrate, only trace amount of M1 was detected in HLM and HLS9 (data not shown). These results indicated that M2, M4 and M5 cannot interconvert with each other. More evidence were needed to validate that M2 and M4 were derived from M1.

Enzymatic Kinetics. Since M1 is aldehyde, M2 is acid and M4 is alcohol, the M1 → M2 + M4 conversion is a dismutase-mediated reaction. To examine the effects of co-factors on this reaction, we characterized the enzymatic kinetics with the presence of either $NADP^+$ or NADPH (Fig. 5). In the HLS9 system (0.1 mg/mL), the final concentration of M1 was within the range of 1~500 μM. When only $NADP^+$ was added, after 6-minute incubation, the oxidation product M2 and reduction product M4 were present, and M2 production was much higher than M4; when NADPH was added, a totally opposite reaction pattern was observed, and the formation of M4 was much more than M2. The four kinetic curves associated with different co-factors and products all displayed non-Michaelis-Menten features. The V_{max} (pmol/min/mg protein) and K_{half} (μM) were calculated for these four kinetics curves (Fig. 5): V_{max} = 2.23, K_{half} = 20.5 ($NADP^+$, M2), V_{max} = 2.92, K_{half} = 729.8 ($NADP^+$, M4) (Fig. 5A-C), V_{max} = 0.53, K_{half} = 52.7 (NADPH, M2), V_{max} = 5.53, K_{half} = 362.5 (NADPH, M4) (Fig. 5D-F). These results suggested that multiple enzymes were involved in both the oxidation and reduction processes.

Taken together, our data suggested that DOXO was firstly catalyzed by one or more microsomal CYP enzymes to produce M1, and M1 was subsequently dismutated to M2 and

M4 by cytosolic enzymes with the presence of $NADP^+$/NADPH. The conversion relationship between DOXO and its major metabolites were shown in Fig. 6.

Discussion

Drug metabolism research primarily focuses on: 1) The structure - metabolism relationship. This usually requires the comparison of a series of compounds sharing the same parental structure to map the characteristic metabolic sites and patterns mediated by a particular enzyme. 2) The sequential metabolic reactions in a metabolic pathway. Starting with a single compound, the metabolism is often composed of a series of metabolic conversions, which might involve multiple enzymes and different metabolic routes, and produce a set of metabolites in sequential. Among the three methylxanthine derivatives, DOXO is featured by its distinct metabolic sites and pathways compared to CA and TP, hence could be considered as a model compound for drug metabolism study.

The current understanding of the metabolic sites for methylxanthine derivatives is majorly from the research of CA and TP metabolism (Nehlig, 2018) . CA metabolism remains one of the earliest models to illustrate the sequential metabolism of methylxanthine derivatives *in vivo* (McKeague et al., 2016). CA is characterized by three methyl groups at the N-1, N-3, and N-7 positions on the methylxanthine skeleton (A and B rings), and the N-3 site is the most labile. Demethylation on each of these three sites produces PX, TB or TP, and further demethylation could still happen on the rest of the methyl sites. Compared to TP, CA carries a methyl group on the N-7 position, which increases the lability of the N-3 site of the A ring. DOXO is featured by the cyclic acetal group (C ring) on the N-7 position, and previous studies have not explored how this substituent group affects the metabolic sites and activity of this compound. Our results demonstrated that, the C ring of DOXO largely changed the key metabolic sites. The metabolism of DOXO predominantly happened on the C ring and produced the six major metabolites of the nine. The other three minor metabolites were derived from demethylation on the A and B rings. In addition, the results of the chemical stability of DOXO showed that M1 formation detected in the incubation system was mediated by enzymatic catalysis. Based

on these evidence, we conclude that the methyl groups on the N-1, N-3 and N-7 positions interact with each other to collectively determine the demethylation pattern of CA, and the cyclic acetal group on the N-7 position dominantly guides the characteristic opening of the C ring of DOXO. The lability of these three compounds is ranked from high to low: DOXO > CA > TP. The lability of DOXO arises from the C ring rather than the A and B rings. This is further supported by the detection of trace amount of M6, M7 and M8 in DOXO metabolism.

Previous studies on DOXO metabolism in human primarily focus on pharmacokinetics *in vivo*, and ETO has been identified as the major product (Matera et al., 2017). However, the understanding of the complete metabolic process, i.e. the DOXO to ETO conversion, is still limited. It's suspected that DOXO might have been intentionally designed as a prodrug of ETO. However, there are no published data available regarding the design of DOXO compound based on our literature search. To fully investigate the DOXO metabolism, a systematic characterization of all metabolites and their conversion relationships using both *in vivo* and *in vitro* systems is required.

In our study, we first characterized the metabolite profiles of DOXO in human liver microsomes, human liver S9 and human blood serum. In HLM, M1 was the predominant metabolite; while in human plasma, M2 and M4 were the major metabolites. In HLS9, the percentage of M1, M2 and M4 was 26%, 25% and 47%, respectively. Therefore, two hypotheses for the sequential metabolism of M1 (TA), M2 (TAA) and M4 (ETO): 1, oxidation: M4 (alcohol) is oxidized to M1 (aldehyde), and M1 continues to be oxidized to M2 (acid); 2, dismutation: M1 (aldehyde) is simultaneously oxidized to M2 (acid) and reduced to M4 (alcohol). In the first scenario, M4 is the intermediate product of metabolism of DOXO, and it should be converted into M1 and M2 in the end. We used M4 as substrate in HLM and HLS9 incubation, and intragastrical administered M4 in SD rat (data not shown). Only trace amount of M4 was reverted to M1, and there was no M2 signal at all. Therefore, M4 was concluded to

be the stable end product in both *in vivo* and *in vitro* systems, which in turn rejected the first hypothesis. The second scenario is that M1 could be directly dismutated into M2 and M4. In HLS9 incubation, we took M1 as substrate, and added NADPH generating system (with a mixture of NADP+ and NADPH) as co-factor. Results showed that M1 was converted to M2 and M4. In addition, we demonstrated that M2 and M4 were not inter-convertible (Fig. 6). Therefore, M1 was validated as the initial metabolite in DOXO metabolism. Additional experiments were conducted to verify that without the formation of the initial metabolite M1, DOXO can hardly be directly metabolized to M2 and M4. We further demonstrated that in HLM and HLS9, the initial metabolism of DOXO was blocked by the broad-spectrum CYP inhibitor These data collectively confirmed the second hypothesis. Moreover, the metabolic rate for the DOXO to M1 conversion in HLM was 222 pmol/mg/min, whereas the rate for the M1 → M2 + M4 conversion in HLS9 was about 2000 pmol/mg/min. HLM is known to be concentrated by nearly 3-fold via centrifugation of HLS9 (Hakooz et al., 2006), therefore the metabolic enzymes converting M1 to M2 and M4 are present in non-HLM fractions of HLS9. The metabolic rate for the M1 → M2 + M4 conversion was roughly 30-fold of that for the DOXO to M1 conversion. Taken together, we concluded that the conversion from DOXO to M1 conversion is the rate-limiting step in DOXO metabolism.

In addition, we also set up HLM mediated reactions in UGT incubation system, using DOXO, M2 and M4 as individual substrate, and we did not find any glucuronidation (SFig. 8).

Aldehyde dismutation is a classical reaction, either spontaneous or catalyzed by dismutase. Our data validated that the dismutation of M1 was enzyme dependent, and it primarily happened in HLS9 with the presence of co-factors (Fig. 4B). Several aldehyde oxidases and reductases might have been involved in this process (Laskar and Younus, 2019). The preliminary experiment on HLS9 kinetics showed that, both oxidized ($NADP^+$) and reduced (NADPH) co-factors could facilitate this dismutation reaction (Fig. 5). The difference was that

the presence of oxidized co-factor $NADP^+$ majorly lead to oxidation product M2, whereas the reduced co-factor NADPH mostly lead to reduction product M4. Eadie-Hofstee plot was used to display the kinetic curves: two curves for the oxidation product M2 shared the similar pattern, although the co-factors were contrast between these two reactions. The same trend was observed for the other two curves for the reduction product M4 (Fig. 5). All these reactions exhibited the non-Michaelis-Menten feature, suggesting that multiple enzymes were involved in this dismutation process.

To summarize, in human liver cells, the initiation of DOXO metabolism relies on the microsomal enzymes, especially CYP and the NADPH. Under pathological conditions, as the NADPH decreases, the initiation of DOXO metabolism, i.e. the formation of M1, could significantly slow down. Whether M1 stays stable or is metabolized to M2 and M4, is determined by the presence of dismutase, and the ratio of $NADP^+$/NADPH in the cytosol (Fig. 5).All these factors could contribute to the pharmacokinetic variability of DOXO among individuals and among different health conditions (Shukla et al., 2009).

In conclusion, in this study we utilized *in vitro* and *in vivo* assay to identify and characterize the initial steps and key metabolites in DOXO metabolism. We systematically investigated the conversion relationships between DOXO and the abundant metabolites M1, M2 and M4. Our results showed that DOXO was firstly metabolized to M1 by CYP enzymes in liver microsomes, and M1 was subsequently converted to M2 and M4 by the dismutase in the cytosol. These findings laid the ground for future studies to elucidate the metabolic pathways of DOXO and the structure-metabolism relationships for methylxanthine derivatives.

Acknowledgements

We thank Dr. Guoliang Chen for the help in synthesis and purification of reference standards (M5), and Dr. Jiangwei Zhang for the support in mass spectrometry analysis. We also acknowledged Dr. Hailing Cheng and Dr. Pixu Liu for the manuscript writing and revision.

Authorship Contributions

Participated in research design: XZ, LY, HM and SX

Conducted experiments: XZ, QP, HM and MM

Contributed new reagents or analytic tools: XZ, QP, LZ, and GG

Performed data analysis: XZ, PS, XQ and LZ

Wrote or contributed to the writing of the manuscript: HW, LY, XZ, HM, QP, and LZ

References

Bertil BF (2010) *Methylxanthines.*Springer, Heidelberg Dordrecht London New York.

Cravanzola C, Reboani MC, Grosa G, and Franzone JS (1989) Doxofylline in rat brain in relation to locomotor activity. *Drug metabolism and disposition: the biological fate of chemicals* **17:**437-440.

Dai ZR, Feng L, Jin Q, Cheng H, Li Y, Ning J, Yu Y, Ge GB, Cui JN, and Yang L (2017) A practical strategy to design and develop an isoform-specific fluorescent probe for a target enzyme: CYP1A1 as a case study. *Chemical science* **8:**2795-2803.

Dai ZR, Ge GB, Feng L, Ning J, Hu LH, Jin Q, Wang DD, Lv X, Dou TY, Cui JN, and Yang L (2015) A Highly Selective Ratiometric Two-Photon Fluorescent Probe for Human Cytochrome P450 1A. *Journal of the American Chemical Society* **137:**14488-14495.

Dini FL and Cogo R (2001) Doxofylline: a new generation xanthine bronchodilator devoid of major cardiovascular adverse effects. *Current medical research and opinion* **16:**258-268.

Fang LN, Mao MQ, Zhao XH, Yang L, Jia H, and Xia SY (2019) Development and validation of a UPLC-MS/MS method for quantification of doxofylline and its metabolites in human plasma. *Journal of pharmaceutical and biomedical analysis* **174:**220-225.

Fort DJ, Stover EL, Propst T, Hull MA, and Bantle JA (1996) Evaluation of the developmental toxicity of theophylline, dimethyluric acid, and methylxanthine metabolites using Xenopus. *Drug Chem Toxicol* **19:**267-278.

Grosa G, Franzone JS, and Biglino G (1986) Metabolism of doxophylline by rat liver microsomes. *Drug metabolism and disposition: the biological fate of chemicals* **14:**267-270.

Hakooz N, Ito K, Rawden H, Gill H, Lemmers L, Boobis AR, Edwards RJ, Carlile DJ, Lake BG, and Houston JB (2006) Determination of a human hepatic microsomal scaling factor for predicting in vivo drug clearance. *Pharmaceutical research* **23:**533-539.

Laskar AA and Younus H (2019) Aldehyde toxicity and metabolism: the role of aldehyde dehydrogenases in detoxification, drug resistance and carcinogenesis. *Drug Metab Rev* **51:**42-64.

Lazzaroni M, Grossi E, and Bianchi Porro G (1990) The effect of intravenous doxofylline or aminophylline on gastric secretion in duodenal ulcer patients. *Alimentary pharmacology & therapeutics* **4:**643-649.

Martinez-Lopez S, Sarria B, Baeza G, Mateos R, and Bravo-Clemente L (2014) Pharmacokinetics of caffeine and its metabolites in plasma and urine after consuming a soluble green/roasted coffee blend by healthy subjects. *Food research international* **64:**125-133.

Matera MG, Page C, and Cazzola M (2017) Doxofylline is not just another theophylline! *Int J Chronic Obstr* **12:**3487-3493.

McKeague M, Wang YH, Cravens A, Win MN, and Smolke CD (2016) Engineering a microbial platform for de novo biosynthesis of diverse methylxanthines. *Metabolic engineering* **38:**191-203.

Mennini FS, Sciattella P, Marcellusi A, Marcobelli A, Russo A, and Caputi AP (2017) Treatment plan comparison in acute and chronic respiratory tract diseases: an observational study of doxophylline vs. theophylline. *Expert review of pharmacoeconomics & outcomes research* **17:**503-510.

Minton NA and Henry JA (1996) Acute and chronic human toxicity of theophylline. *Human & experimental toxicology* **15:**471-481.

Nehlig A (2018) Interindividual Differences in Caffeine Metabolism and Factors Driving Caffeine Consumption. *Pharmacological reviews* **70:**384-411.

Rodopoulos N and Norman A (1997) Elimination of theophylline metabolites in healthy adults. *Scandinavian journal of clinical and laboratory investigation* **57:**233-240.

Rogliani P, Calzetta L, Ora J, Cazzola M, and Matera MG (2019) Efficacy and safety profile of doxofylline compared to theophylline in asthma: a meta-analysis. *Multidisciplinary respiratory medicine* **14:**25.

Sacco C, Braghiroli A, Grossi E, and Donner CF (1995) The effects of doxofylline versus theophylline on sleep architecture in COPD patients. *Monaldi archives for chest disease = Archivio Monaldi per le malattie del torace* **50:**98-103.

Sharma PL and Sharma RM (1979) Comparative bioavailability of sustained-release and conventional tablets of hydroxyethyltheophylline in man. *International journal of clinical pharmacology and biopharmacy* **17:**394-396.

Shukla D, Chakraborty S, Singh S, and Mishra B (2009) Doxofylline: a promising methylxanthine derivative for the treatment of asthma and chronic obstructive pulmonary disease. *Expert opinion on pharmacotherapy* **10:**2343-2356.

Shum LY and Jusko WJ (1987) Theophylline tissue partitioning and volume of distribution in normal and dietary-induced obese rats. *Biopharmaceutics & drug disposition* **8:**353-364.

Spina D and Page CP (2017) Xanthines and Phosphodiesterase Inhibitors. *Handbook of experimental pharmacology* **237:**63-91.

Tanikawa K, Matsumoto Y, Matsuzaki T, Matsumoto M, Fukuoka M, Noguchi S, and Goshima T (1999) Population pharmacokinetic analysis of theophylline: Relationship between serum concentrations and clinical effects in therapeutic drug monitoring. *Yakugaku Zasshi* **119:**861-867.

Troger U and Meyer FP (1995) Influence of endogenous and exogenous effectors on the pharmacokinetics of theophylline. Focus on biotransformation. *Clinical pharmacokinetics* **28:**287-314.

van Mastbergen J, Jolas T, Allegra L, and Page CP (2012) The mechanism of action of doxofylline is unrelated to HDAC inhibition, PDE inhibition or adenosine receptor antagonism. *Pulm Pharmacol Ther* **25:**55-61.

Footnotes

This work was supported by the National Key Research and Development Program of China (2017YFC1702000, 2017YFC1700200), NSF of China (81773810, 81922070, 81973393), and the Key Science and Technology Program of Shenyang supported by Shenyang Science and Technology Bureau (17-230-9-05).

Figure Legends

Fig. 1. Schematic diagram of skeleton of methylxanthine derivatives.

Fig. 2. Main metabolites of DOXO in liver microsomes of different species (HLM, MLM, RaLM, RLM and CyLM). Results are shown as the mean (n = 3).

Fig. 3. Drug concentration-time curve of prototype and metabolites of DOXO after i.v. drip of 100 mg DOXO in the plasma samples of 3 healthy human subjects.

Fig. 4. Metabolism of DOXO and major metabolite M1 in HLM and HLS9. Results are shown as the mean (n = 2). (A) The effects of CYP broad-spectrum inhibitor 1-ABT and NADPH-regenerating system on DOXO metabolism in HLM/HLS9 incubation system, and DOXO metabolism with the presence of NADPH-regenerating system only. (B) The effects of CYP broad-spectrum inhibitor 1-ABT and NADPH-regenerating system on M1 metabolism in HLM/HLS9 incubation system, and M1 metabolism with the presence of NADPH-regenerating system only.

*Incubation procedures followed SOP for phase I metabolism *in vitro* incubation.

Fig. 5. The enzyme kinetics analysis and Eadie−Hofstee plot of M1 dismutation to M2 and M4 in HLS9 with the presence of either $NADP^+$ or NADPH. (A) The enzyme kinetic curve of M1 react with $NADP^+$ in HLS9, (B and C) and the Eadie-Hofstee plots of M2 and M4 of $NADP^+$, respectively. (D) The enzyme kinetic curve of M1 react with NADPH in HLS9, (E and F) and the Eadie-Hofstee plots of M2 and M4 of NADPH, respectively.

Fig. 6. Schematics of the relationship between the interconversion of DOXO and its main metabolites. (No known metabolites or DOXO were detected when M2 or M5 was used as a substrate at 100 μM) (SER, smooth endoplasmic reticulum)

--------► metabolic conversion rate < 0.1%

——► 0.1% < metabolic conversion rate <1%

⟹ 1% <metabolic conversion rate < 10%

DMD Fast Forward. Published on February 21, 2020 as DOI: 10.1124/dmd.119.089565
This article has not been copyedited and formatted. The final version may differ from this version.

⟹ metabolic conversion rate > 20%

DMD Fast Forward. Published on February 21, 2020 as DOI: 10.1124/dmd.119.089565
This article has not been copyedited and formatted. The final version may differ from this version.

Fig. 1.

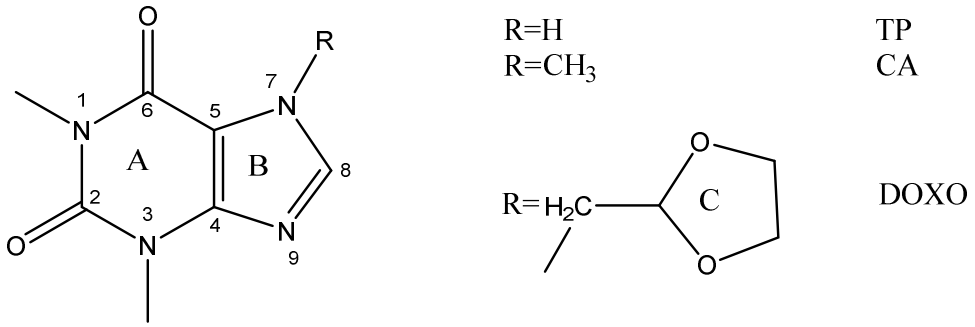

Fig. 2.

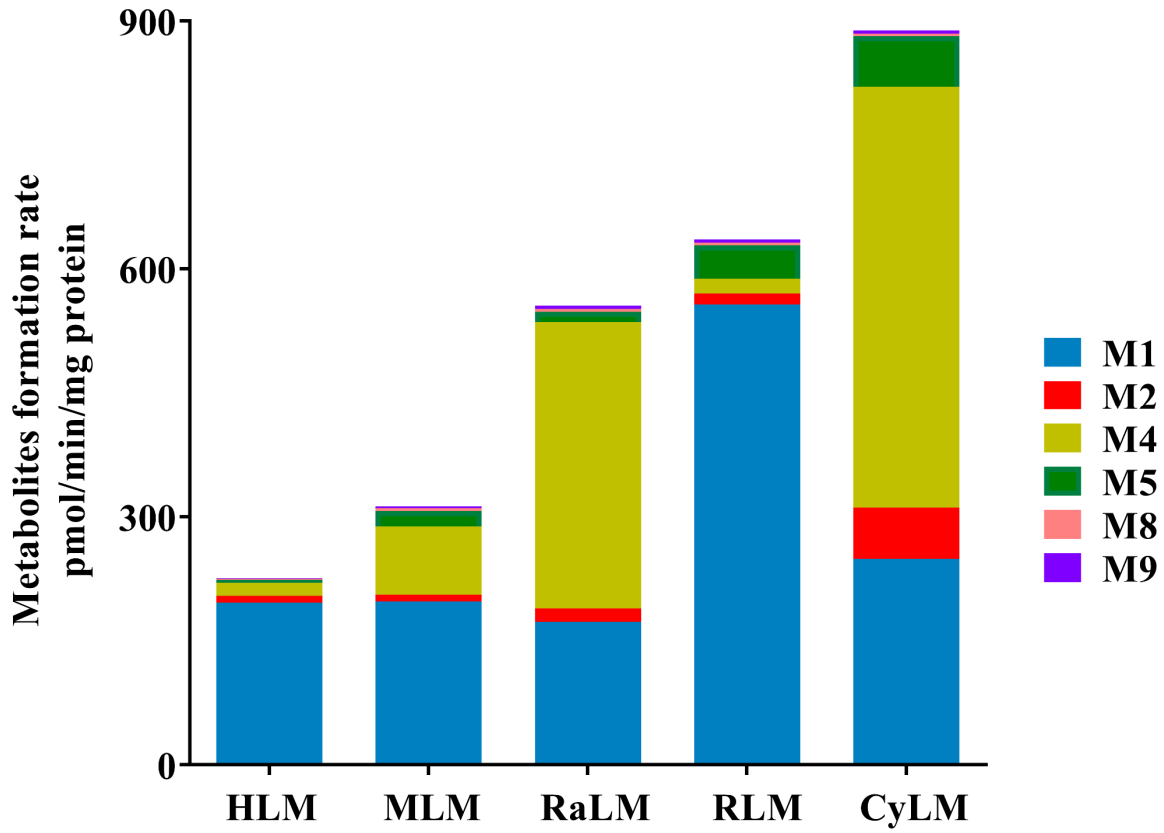

DMD Fast Forward. Published on February 21, 2020 as DOI: 10.1124/dmd.119.089565
This article has not been copyedited and formatted. The final version may differ from this version.

Fig. 3.

A

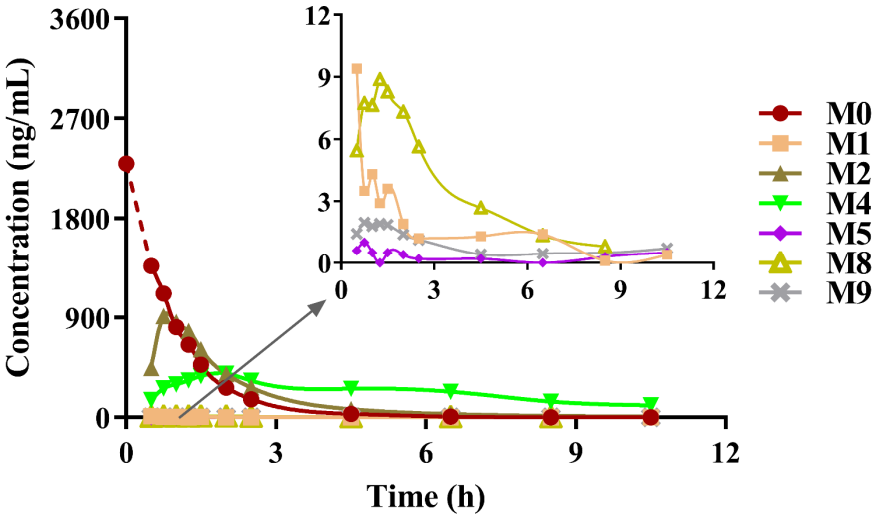

B

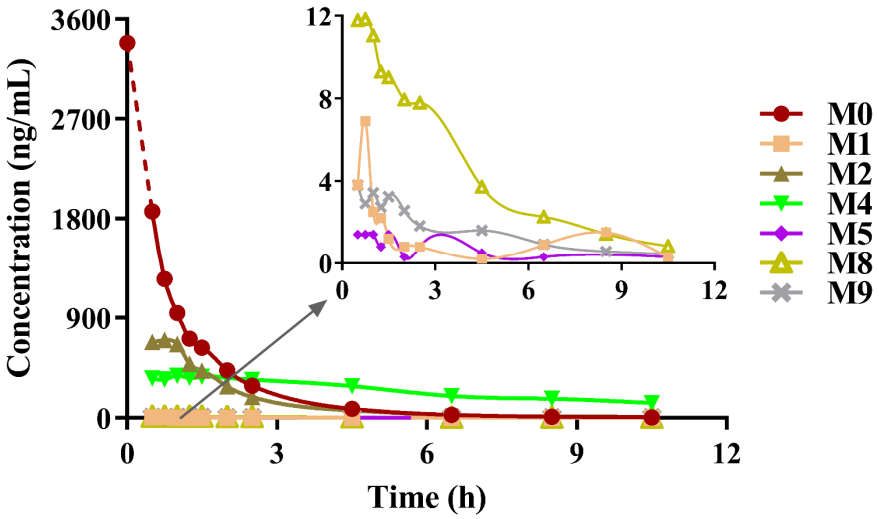

C

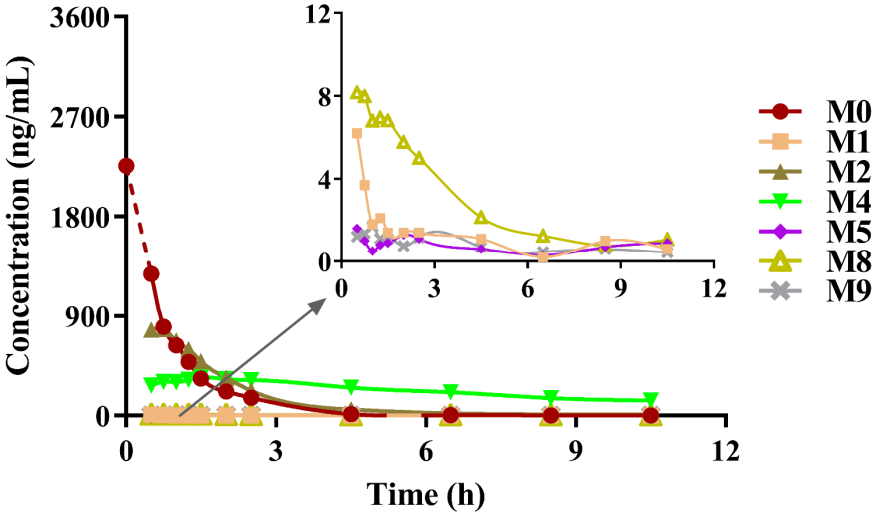

DMD Fast Forward. Published on February 21, 2020 as DOI: 10.1124/dmd.119.089565
This article has not been copyedited and formatted. The final version may differ from this version.

Fig. 4.

A

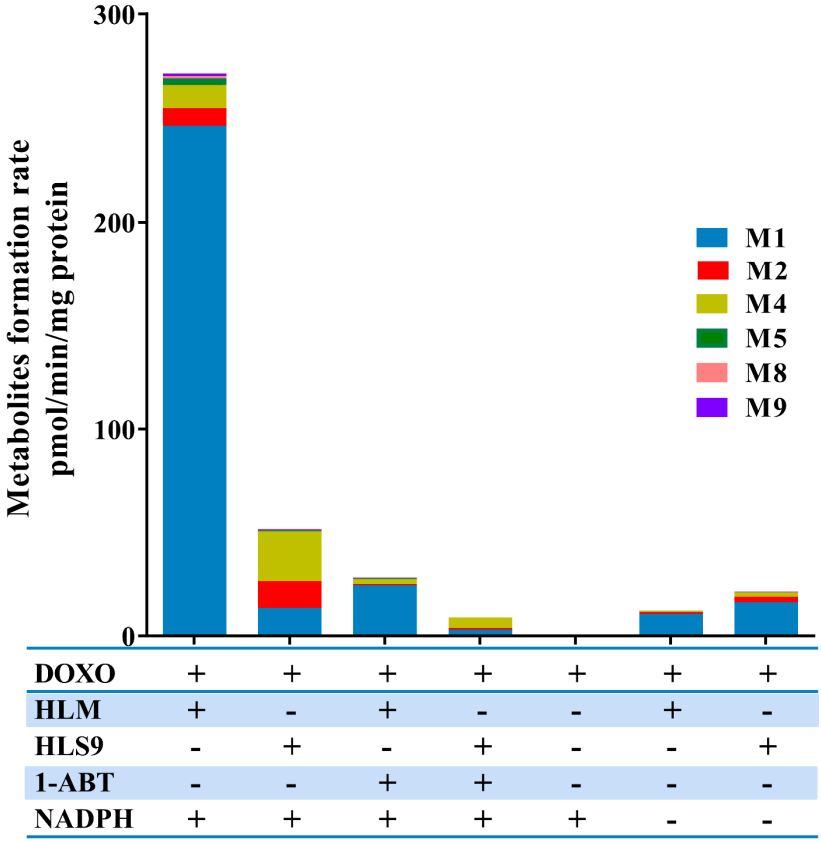

DOXO	+	+	+	+	+	+	+
HLM	+	-	+	-	-	+	-
HLS9	-	+	-	+	-	-	+
1-ABT	-	-	+	+	-	-	-
NADPH	+	+	+	+	+	-	-

B

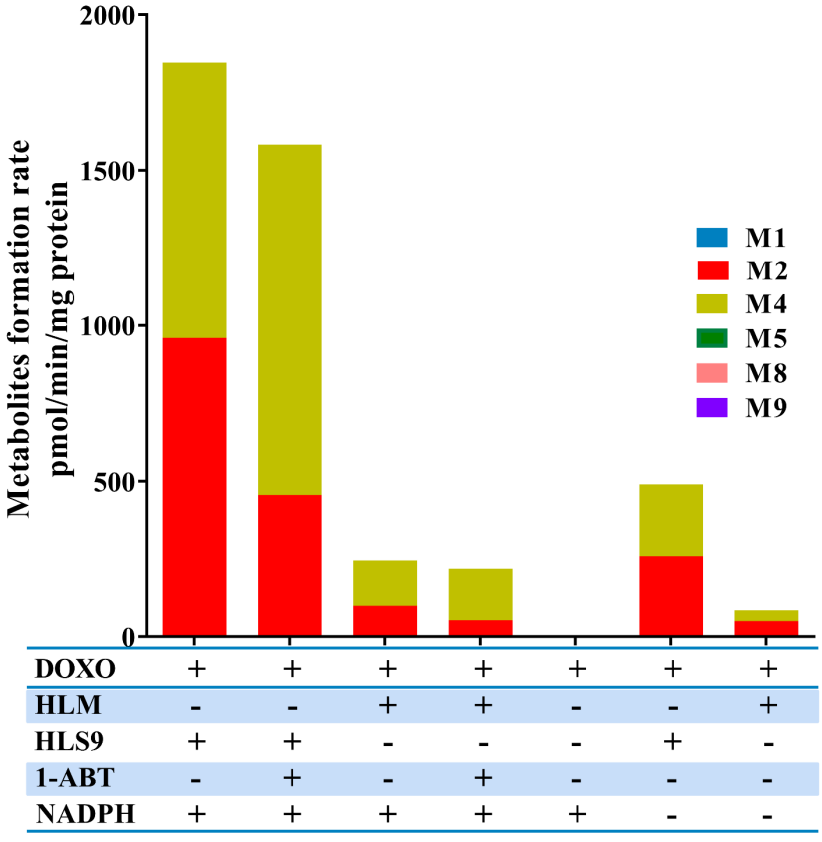

DOXO	+	+	+	+	+	+	+
HLM	-	-	+	+	-	-	+
HLS9	+	+	-	-	-	+	-
1-ABT	-	+	-	+	-	-	-
NADPH	+	+	+	+	+	-	-

Fig. 5.

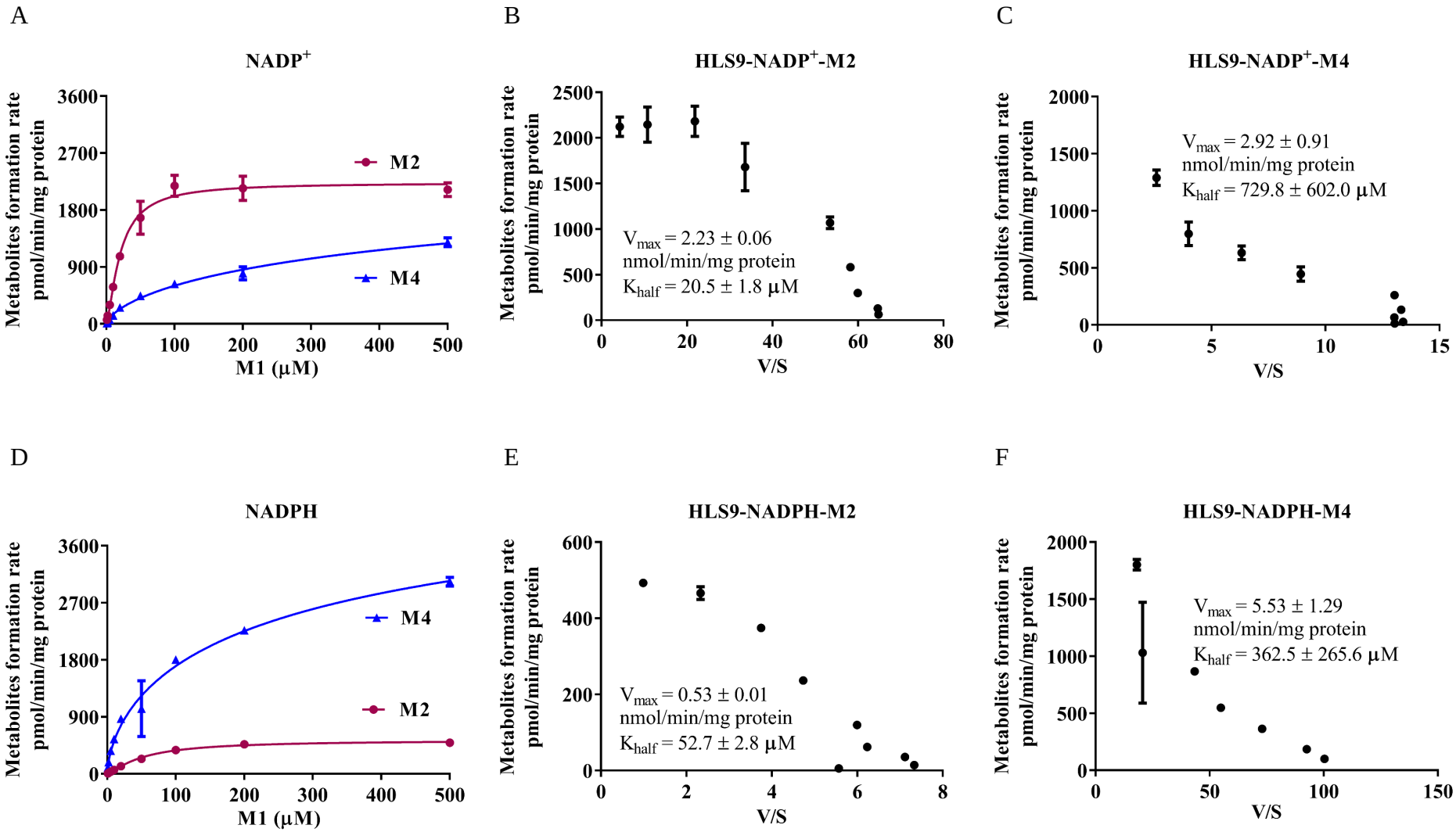

Fig. 6.

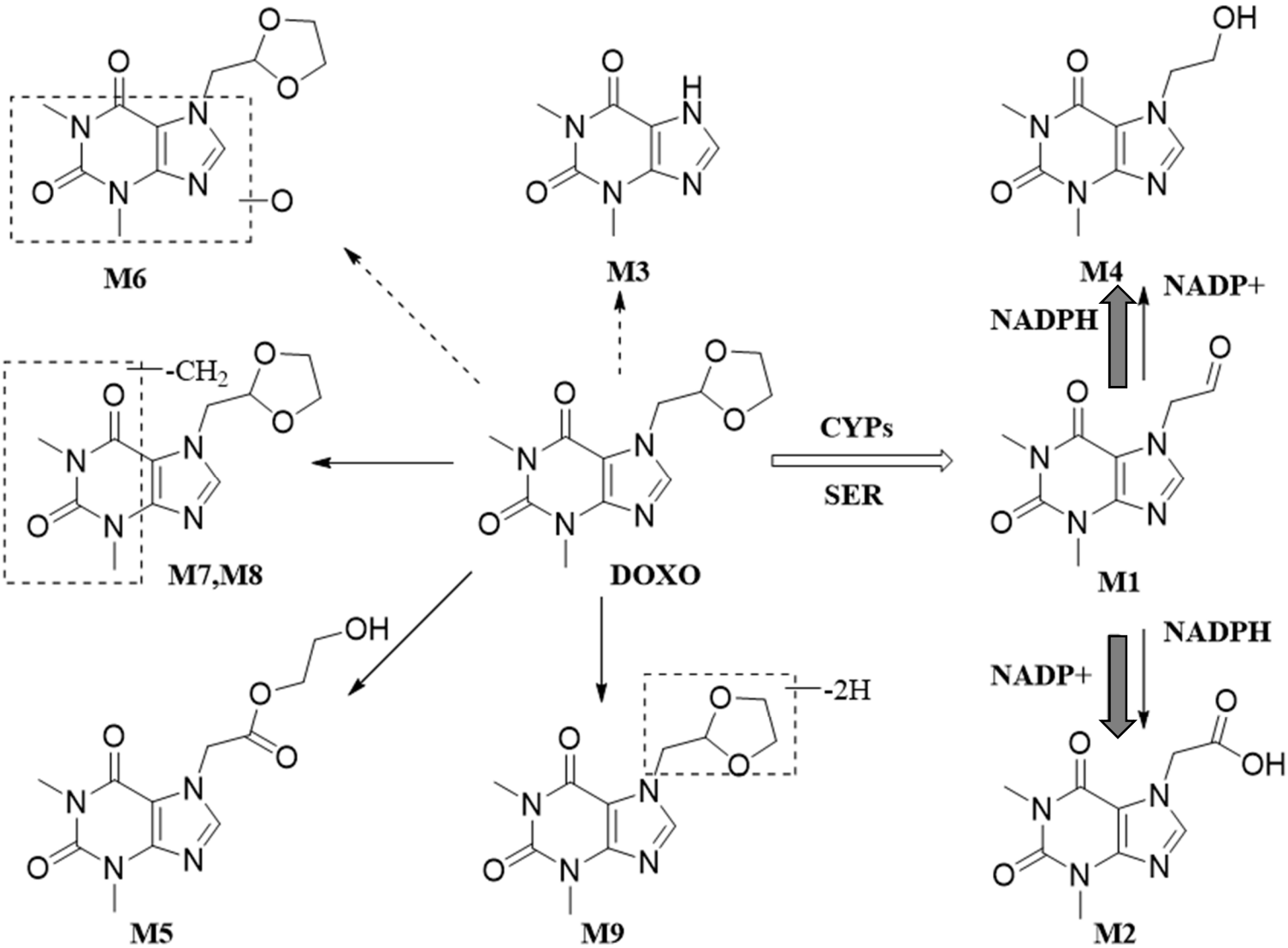

Supplemental Data for

Theophylline acetaldehyde as the initial product in doxophylline metabolism in human liver

Xiaohua Zhao[1,2], Hong Ma[3,4], Qiusha Pan[1,2], Haiyi Wang[1,2], Xingkai Qian[1,2], Peifang Song[1,2], Liwei Zou[1,2], Mingqing Mao[5], Shuyue Xia[5], Guangbo Ge[1,2], Ling Yang[1,2*]

[1]Institute of Interdisciplinary Integrative Medicine Research, Shanghai University of Traditional Chinese Medicine, Shanghai 201203, China

[2]Center for Systems Pharmacokinetics, Shanghai University of Traditional Chinese Medicine, Shanghai 201203, China

[3]College of Basic Medical Sciences, Dalian Medical University, Liaoning 116044, China

[4]Shanghai Research Institute of Acupuncture and Meridian, Shanghai 200030, China

[5]Respiratory Medicine Department, Central Hospital Affiliated to Shenyang Medical College, Liaoning 110034, China

Supplemental Figure

A

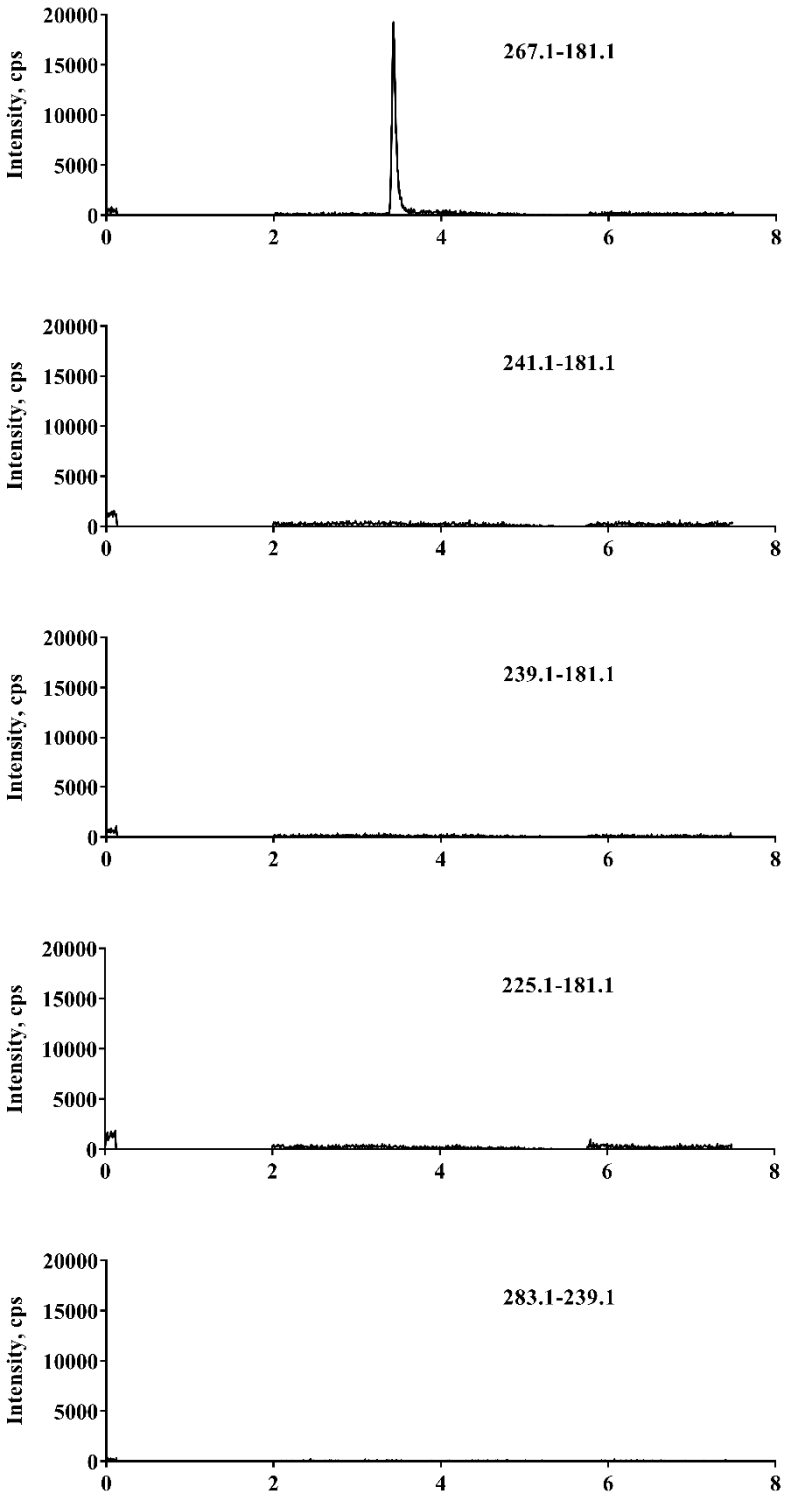

SFig. 1 Representative MRM chromatograms for DOXO and metabolites.

(A) DOXO solution (100 ng/mL)

B

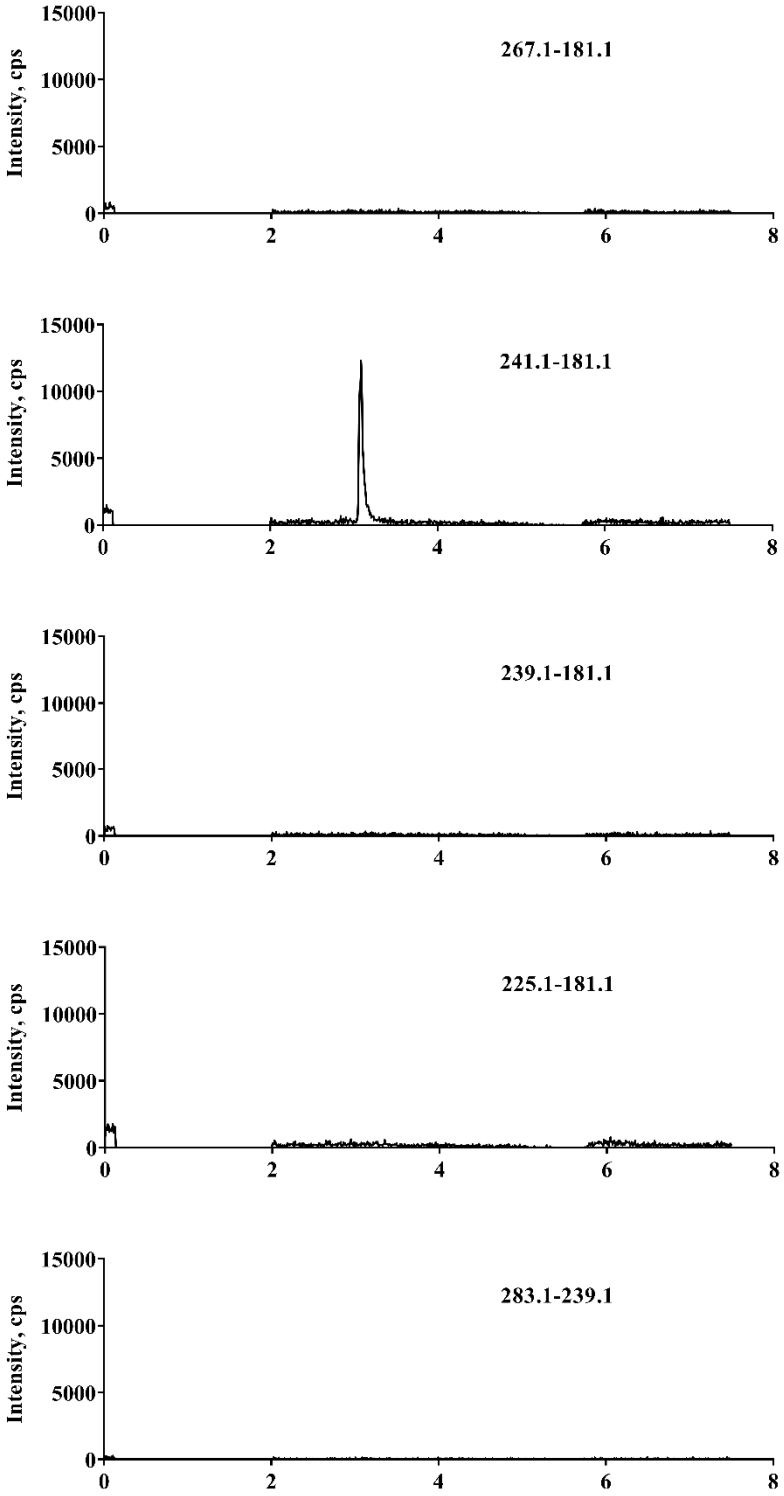

SFig. 1 Representative MRM chromatograms for DOXO and metabolites.

(B) M1 solution (100 ng/mL)

C

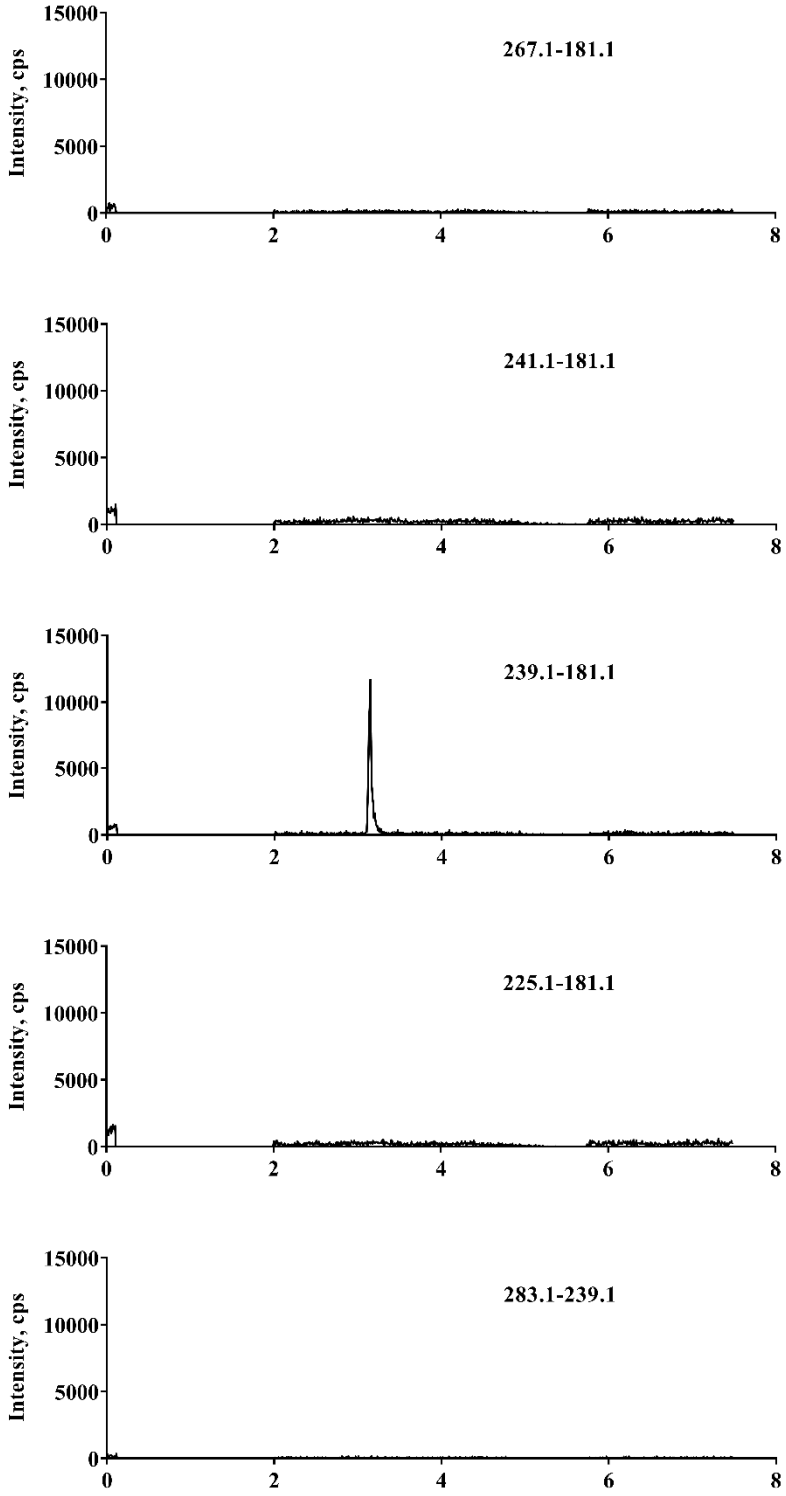

SFig. 1 Representative MRM chromatograms for DOXO and metabolites.

(C) M2 solution (100 ng/mL)

D

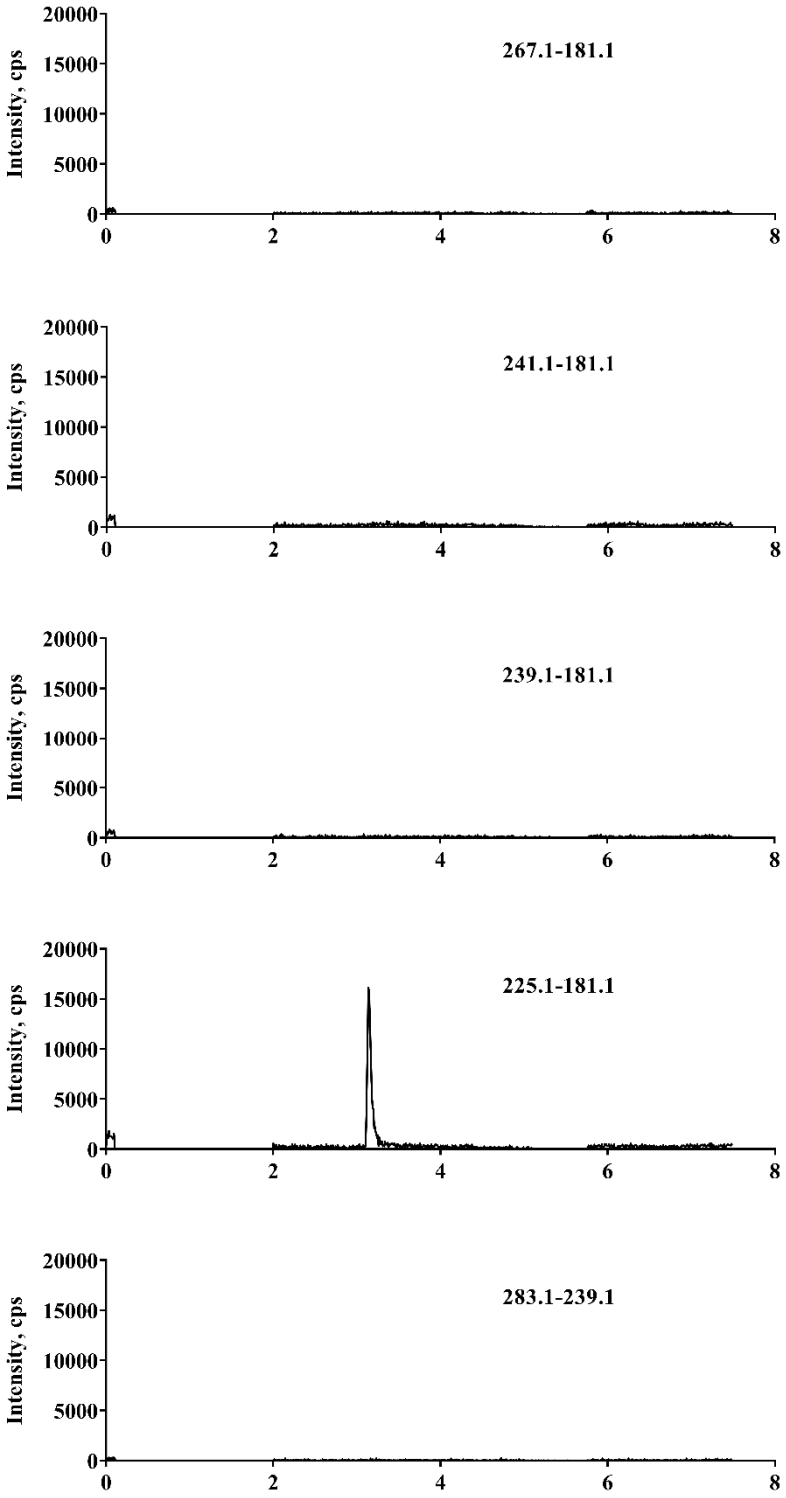

SFig. 1 Representative MRM chromatograms for DOXO and metabolites.

(D) M4 solution (100 ng/mL)

E

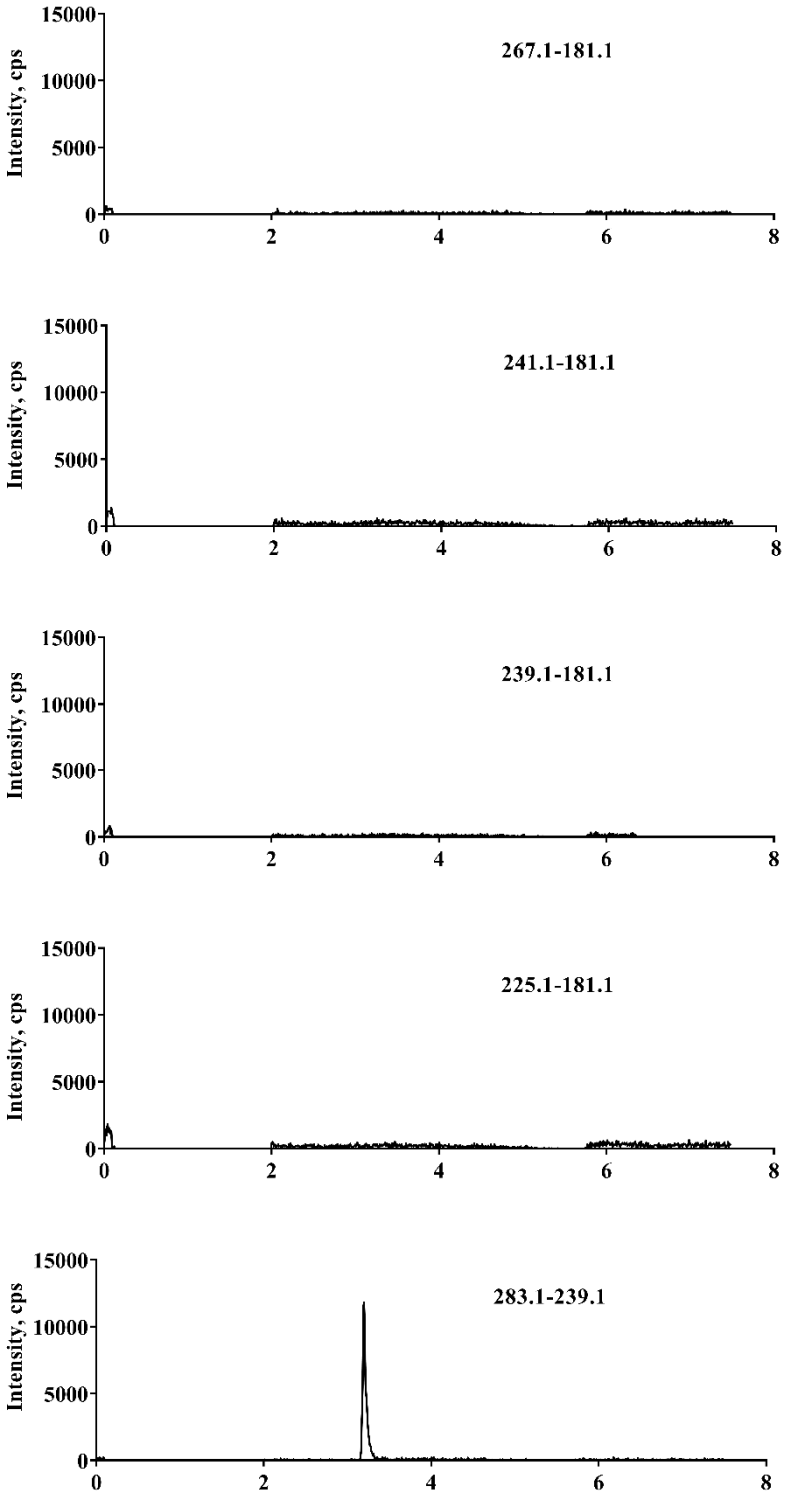

SFig. 1 Representative MRM chromatograms for DOXO and metabolites.

(E) M5 solution (100 ng/mL)

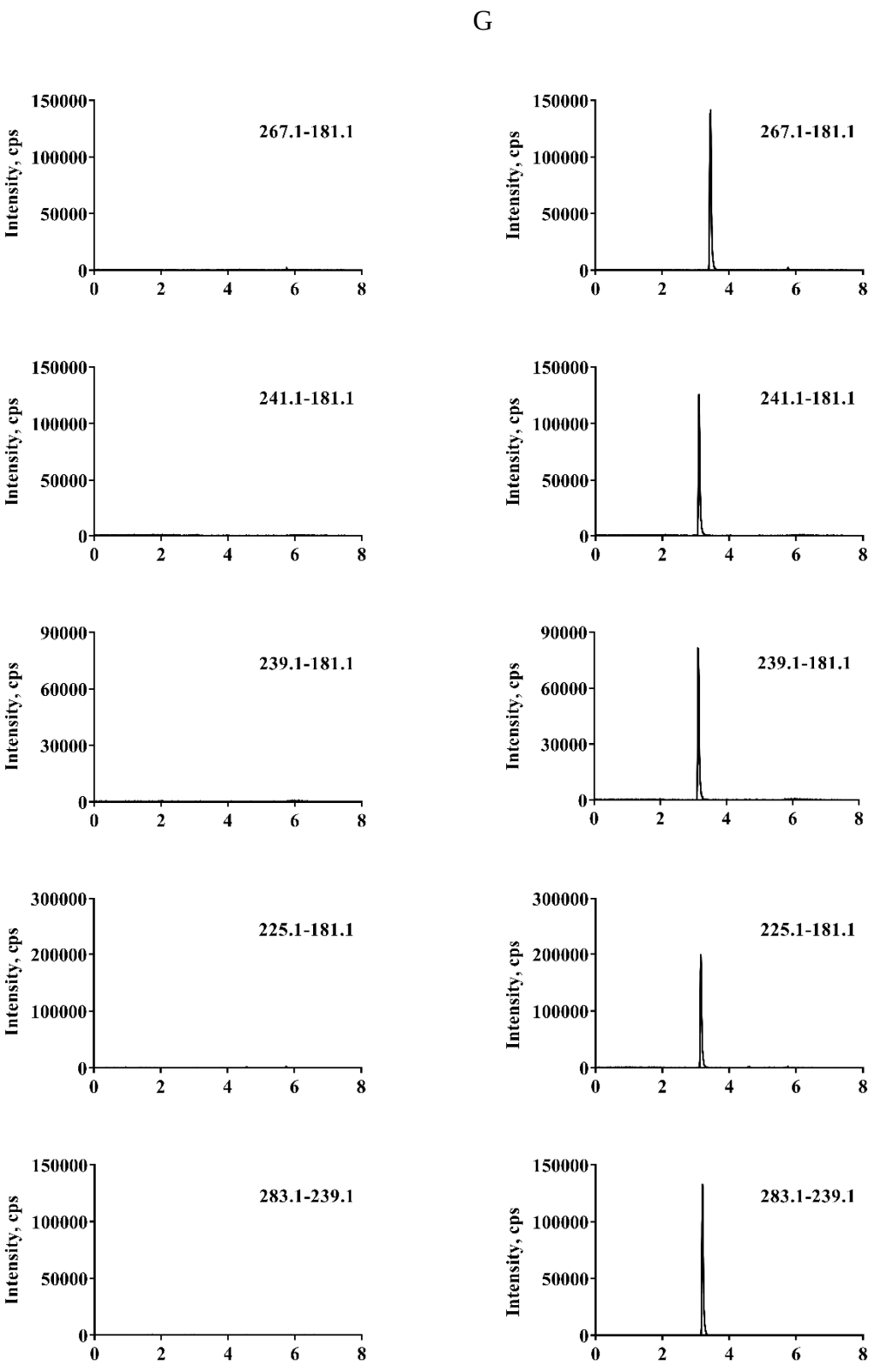

SFig. 1 Representative MRM chromatograms for DOXO and metabolites.
(F) HLM incubation, blank sample (without DOXO); (G) HLM incubation, blank sample spiked with mixture of DOXO, M1, M2, M4 and M5 (final concentration: 100 ng/ml each);

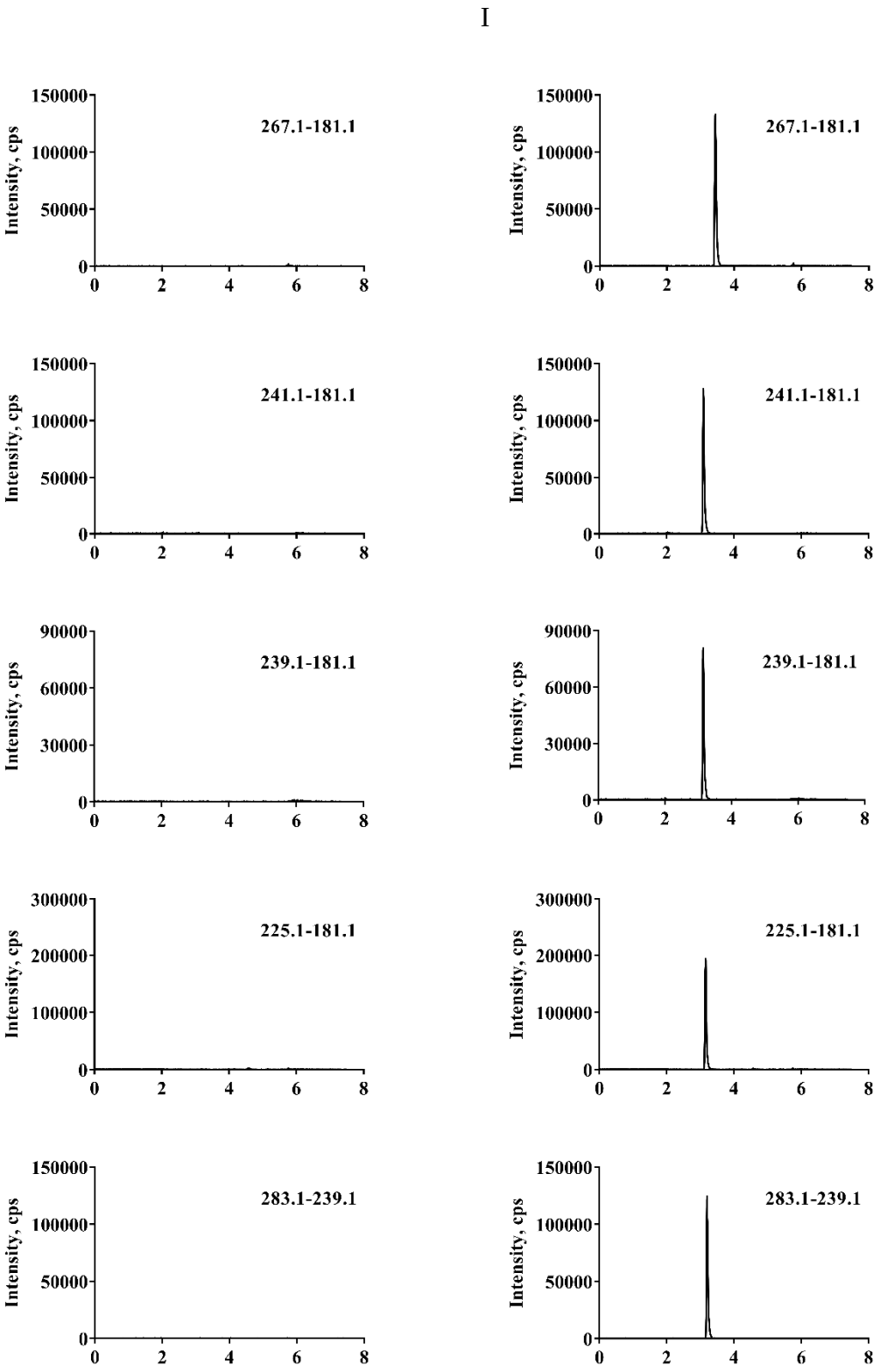

SFig. 1 Representative MRM chromatograms for DOXO and metabolites.
(H) HLS9 incubation, blank sample (without DOXO); (I) HLS9 incubation, blank sample spiked with mixture of DOXO, M1, M2, M4 and M5 (final concentration: 100 ng/ml each);

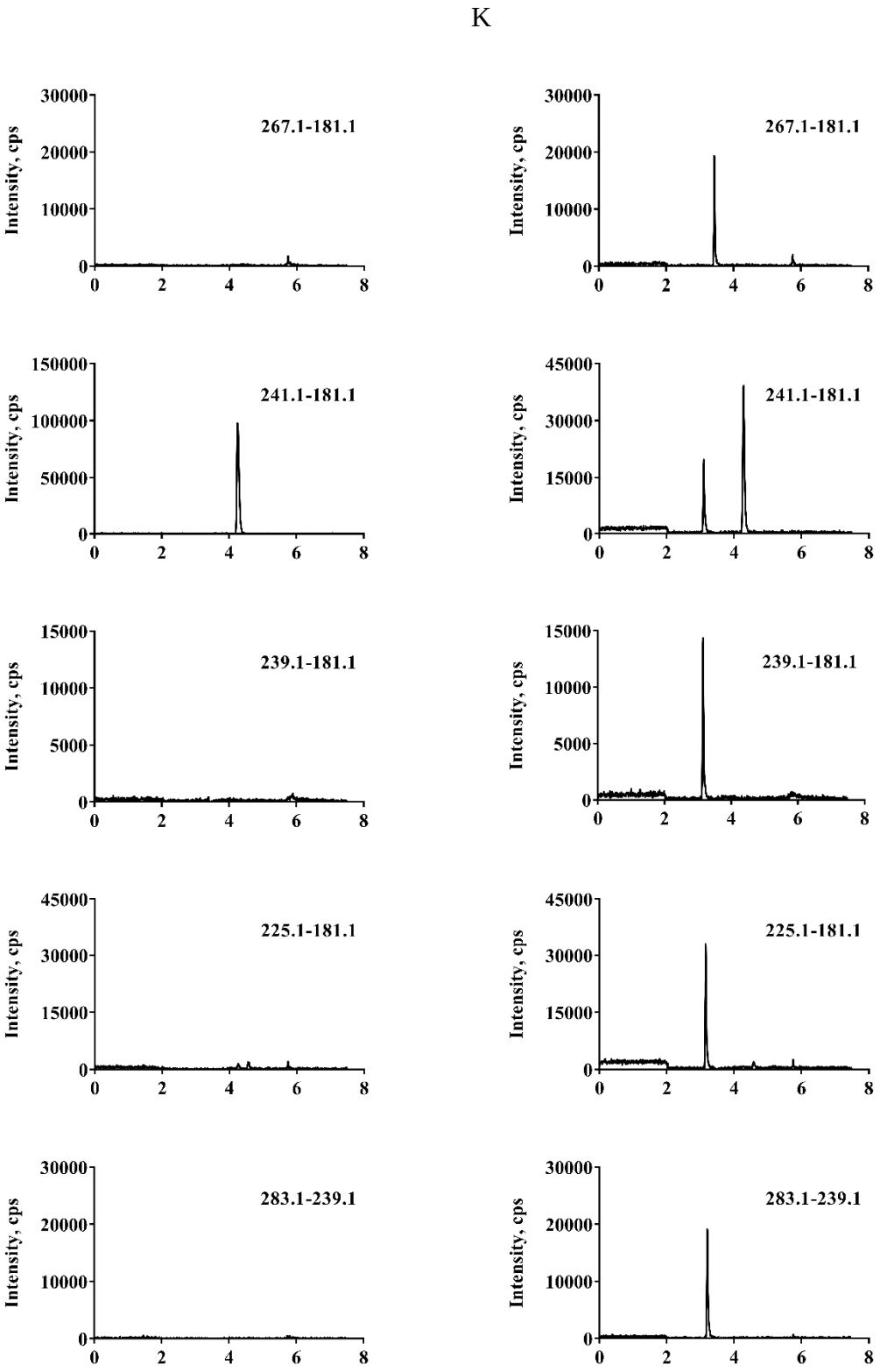

SFig. 1 Representative MRM chromatograms for DOXO and metabolites.
(J) Plasma, blank sample (non-DOXO treated),
(K) Plasma, blank sample spiked with mixture standards of DOXO, M1, M2, M4 and M5 (final plasma concentration: 100 ng/ml each).

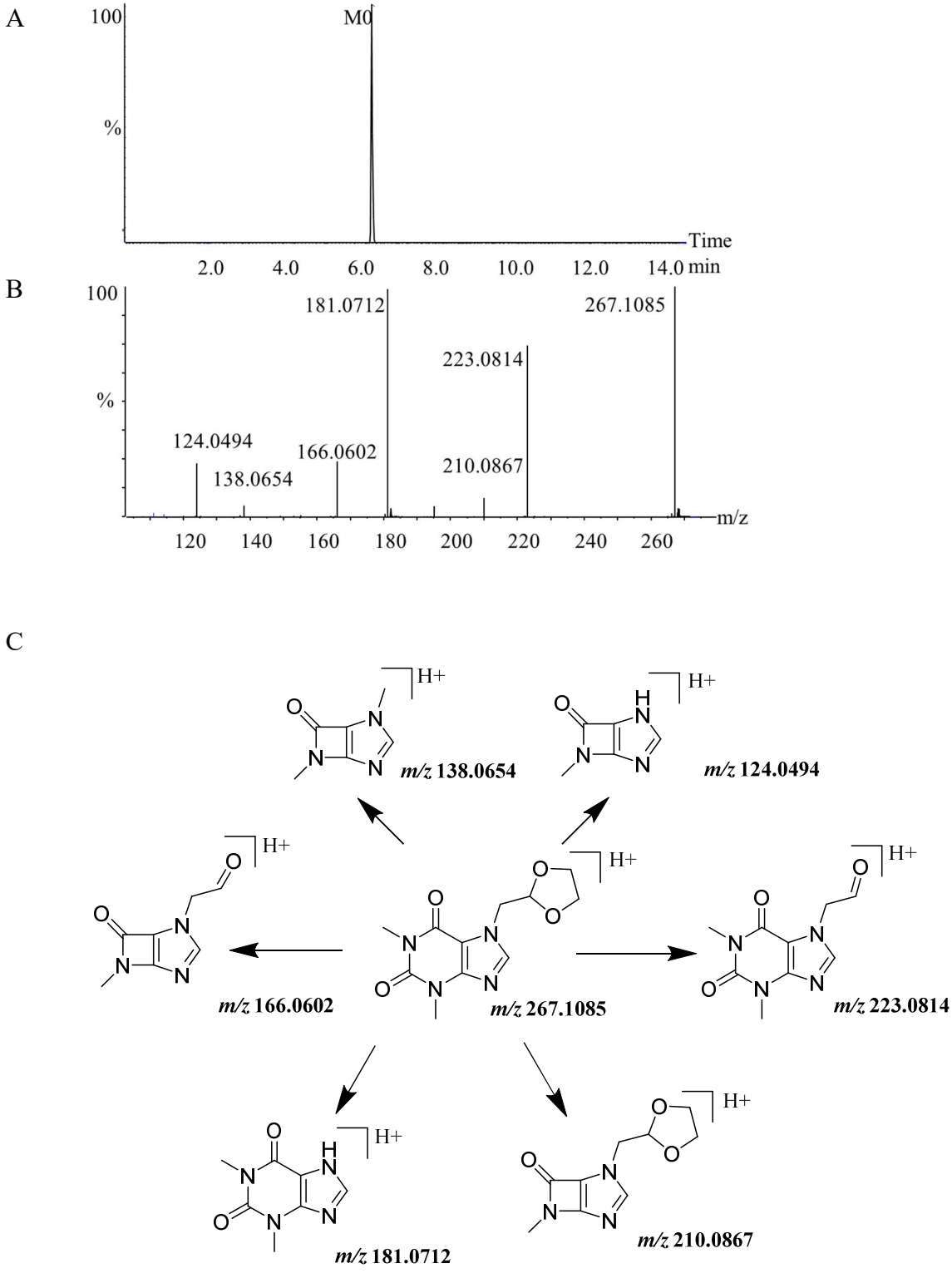

SFig. 2. Chromatography - Mass Spectrometry of DOXO obtained on LC-Triple TOF.
(A) Chromatographic graph of DOXO;
(B) MS^2 spectrum of DOXO in the positive ion mode.
(C) Tentative structural illustration of the most informative fragment ions for DOXO.

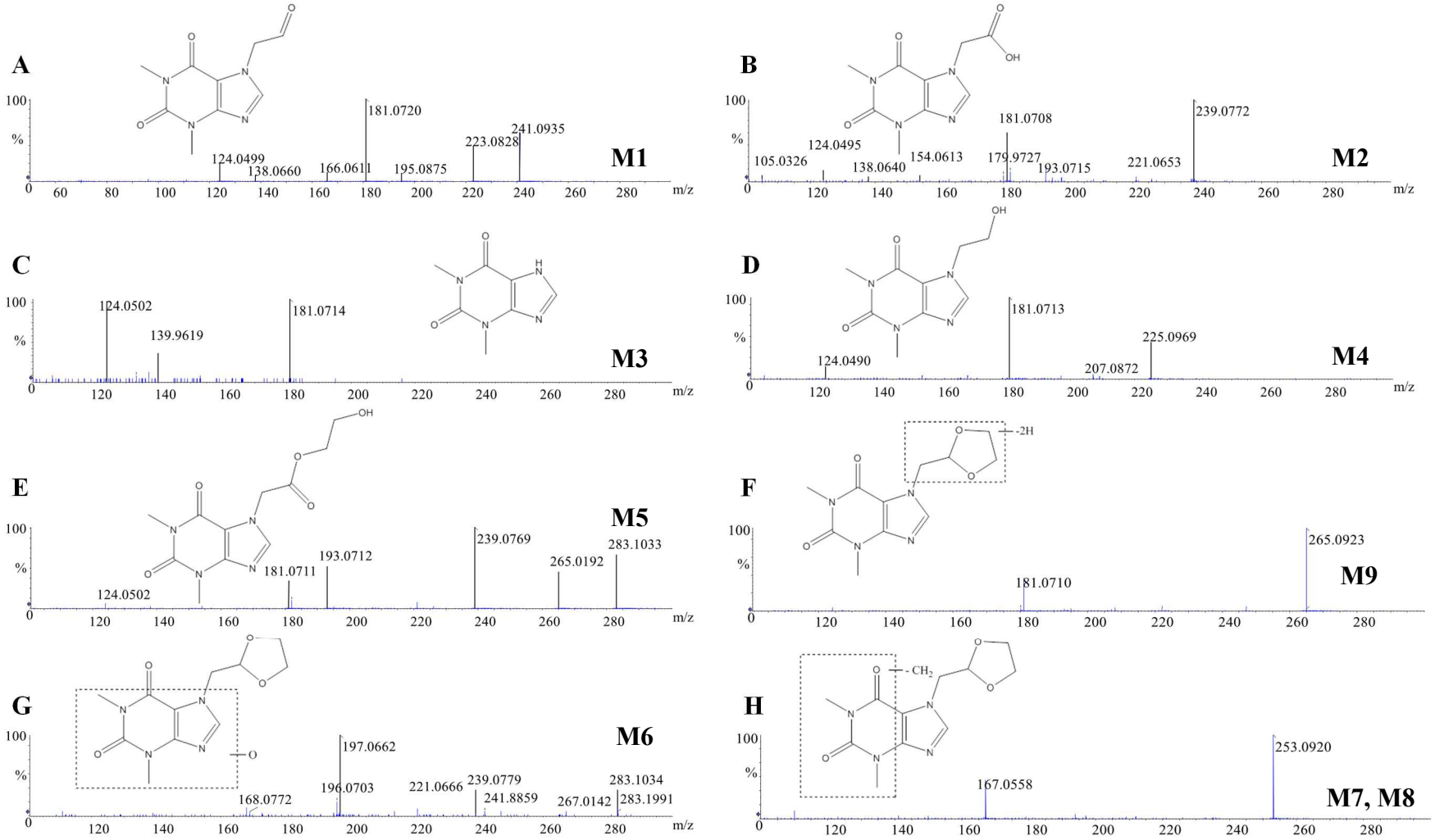

SFig. 3. The MS2 spectra of representative metabolites in HLM. (A) M1; (B) M2; (C) M3; (D) M4; (E) M5; (F) M9; (G) M6; (H) M7 and M8.

SFig. 4.

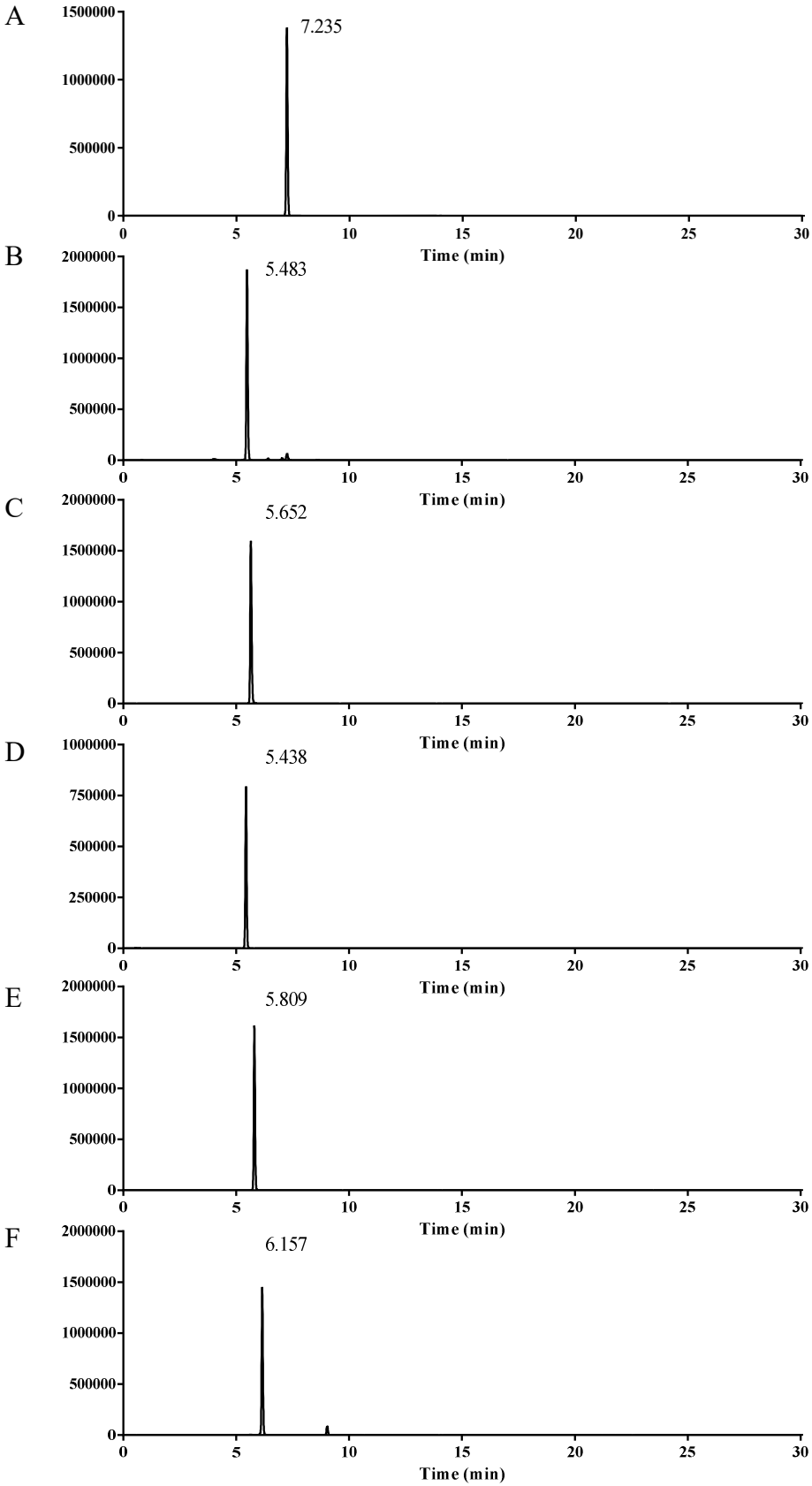

SFig. 4. Chromatography of purity test for reference standards used in the study.
(A) DOXO; (B) M1; (C) M2; (D) M3; (E) M4; (F) M5.

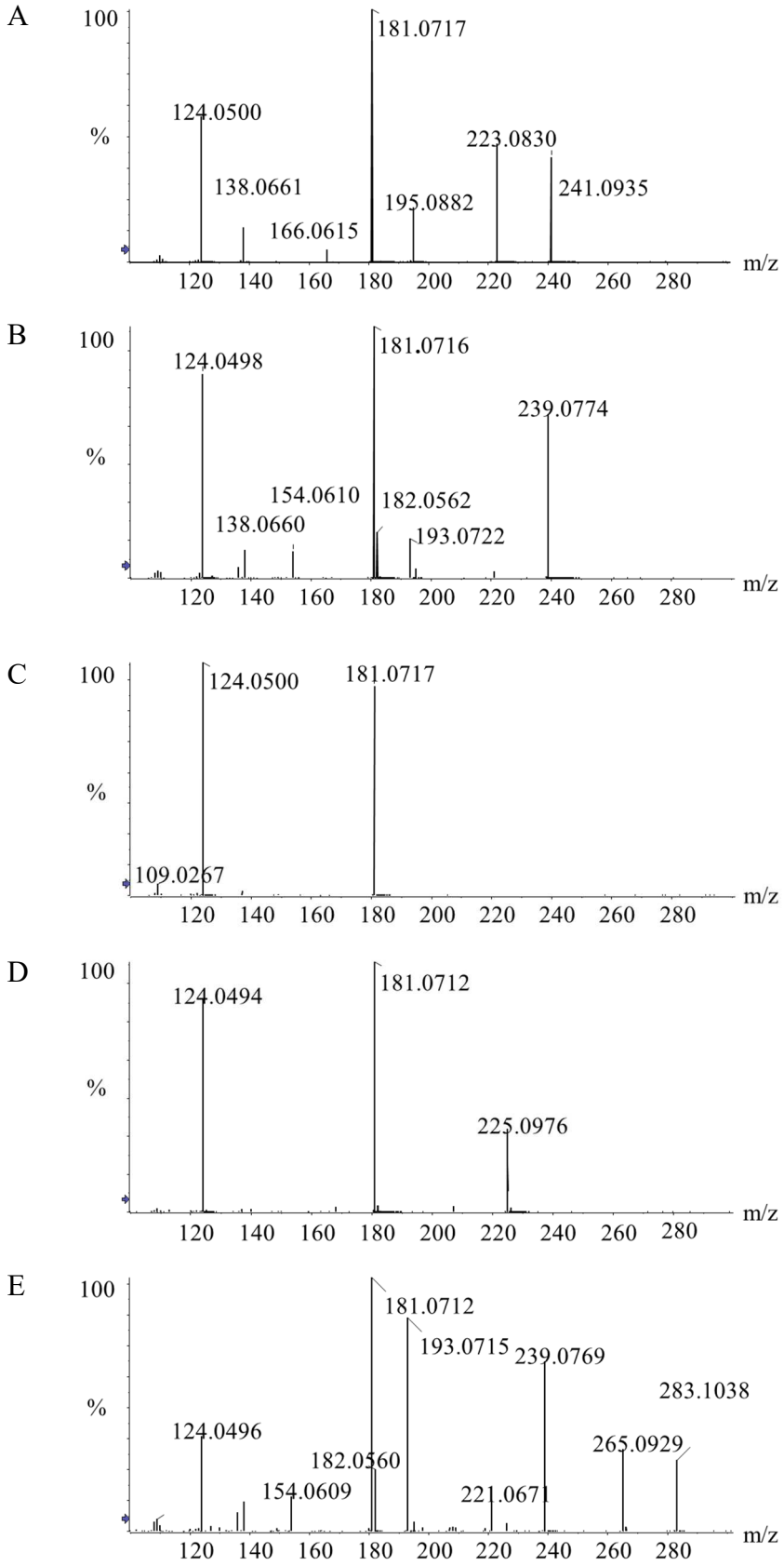

SFig. 5. The MS^2 spectra for reference standards obtained on LC-Triple TOF.
(A) M1; (B) M2; (C) M3; (D) M4; (E) M5.

A

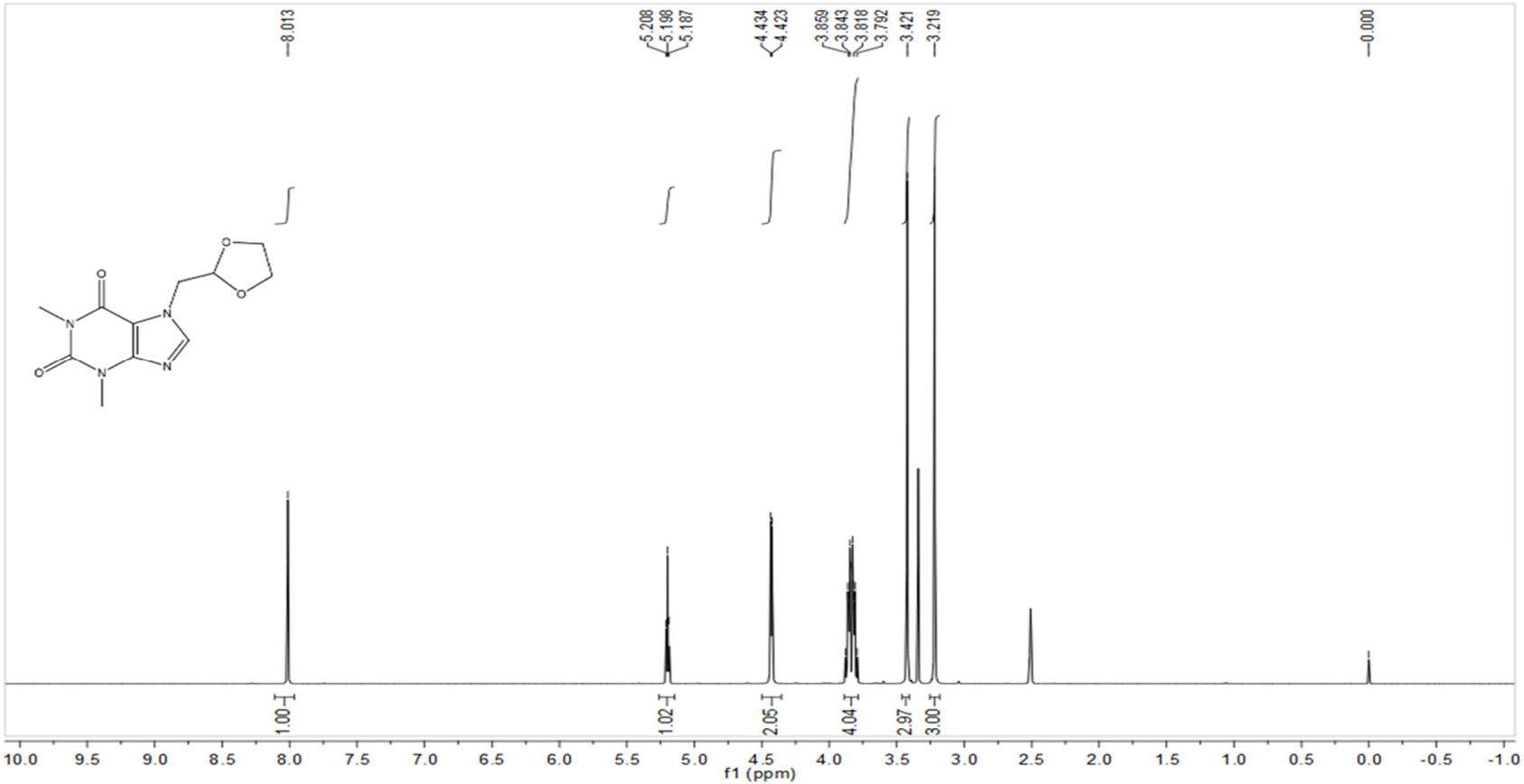

^{1}H NMR (400 MHz, DMSO) δ 8.01 (s, 1H), 5.20 (t, J = 4.2 Hz, 1H), 4.43 (d, J = 4.2 Hz, 2H), 3.84 (m, 4H), 3.42 (s, 3H), 3.22 (s, 3H).

SFig. 6. The ^{1}H-NMR for reference standards. (A) DOXO

B

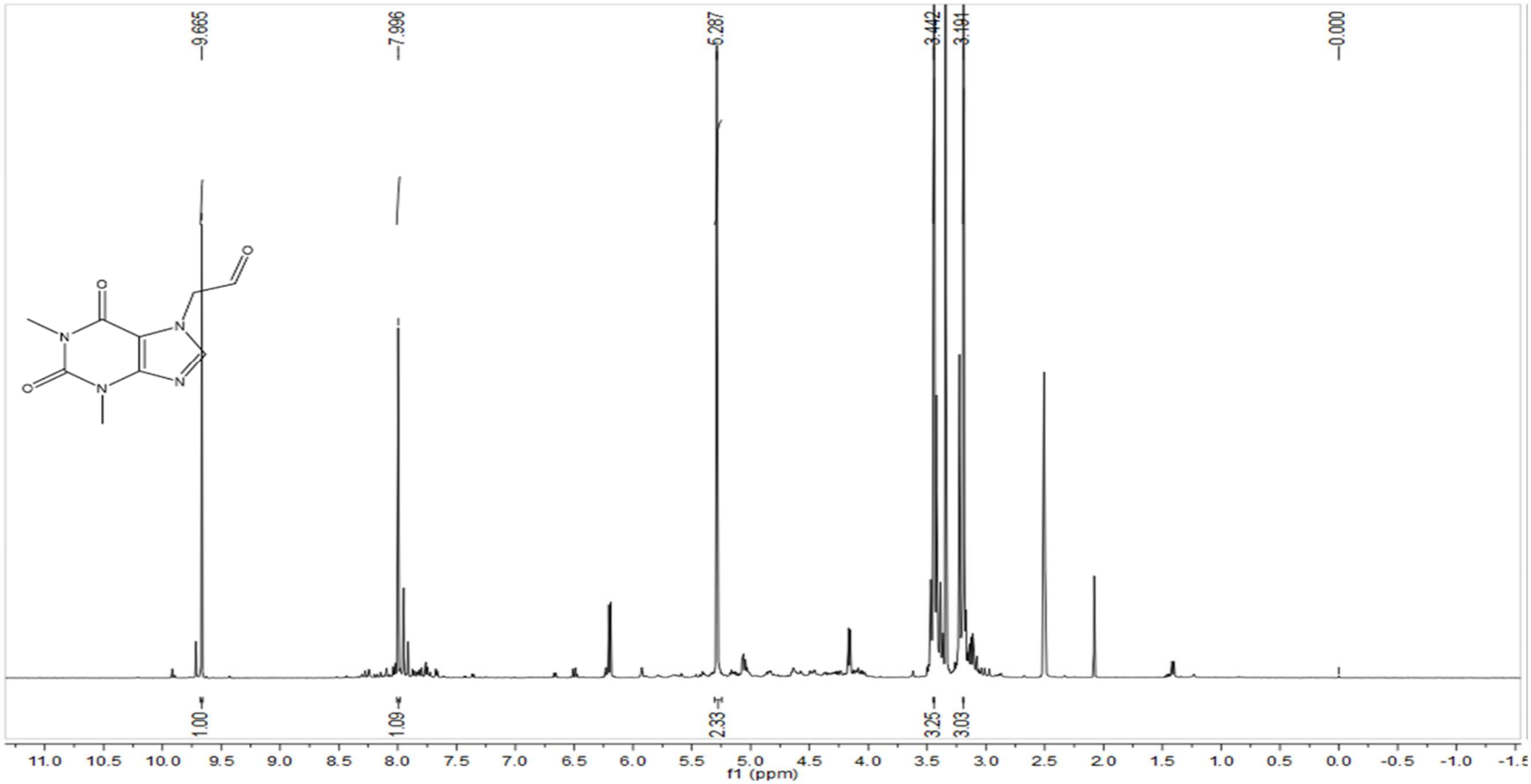

^{1}H NMR (400 MHz, DMSO) δ 9.67 (s, 1H), 8.00 (s, 1H), 5.29 (s, 2H), 3.44 (s, 3H), 3.19 (s, 3H).

SFig. 6. The ^{1}H-NMR for reference standards. (B) M1;

C

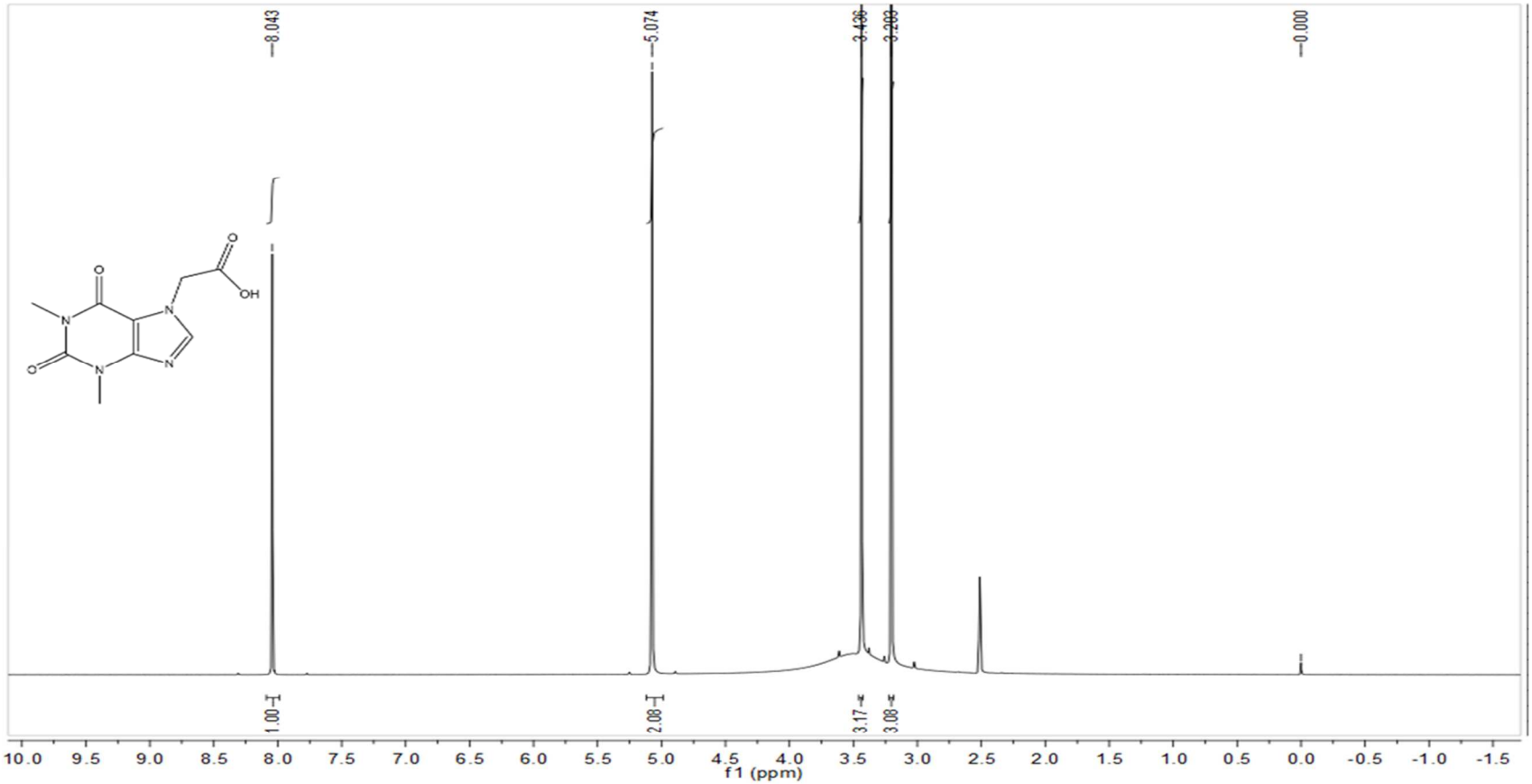

^{1}H NMR (400 MHz, DMSO) δ 8.04 (s, 1H), 5.07 (s, 2H), 3.44 (s, 3H), 3.20 (s, 3H).

SFig. 6. The ^{1}H-NMR for reference standards. (C) M2;

D

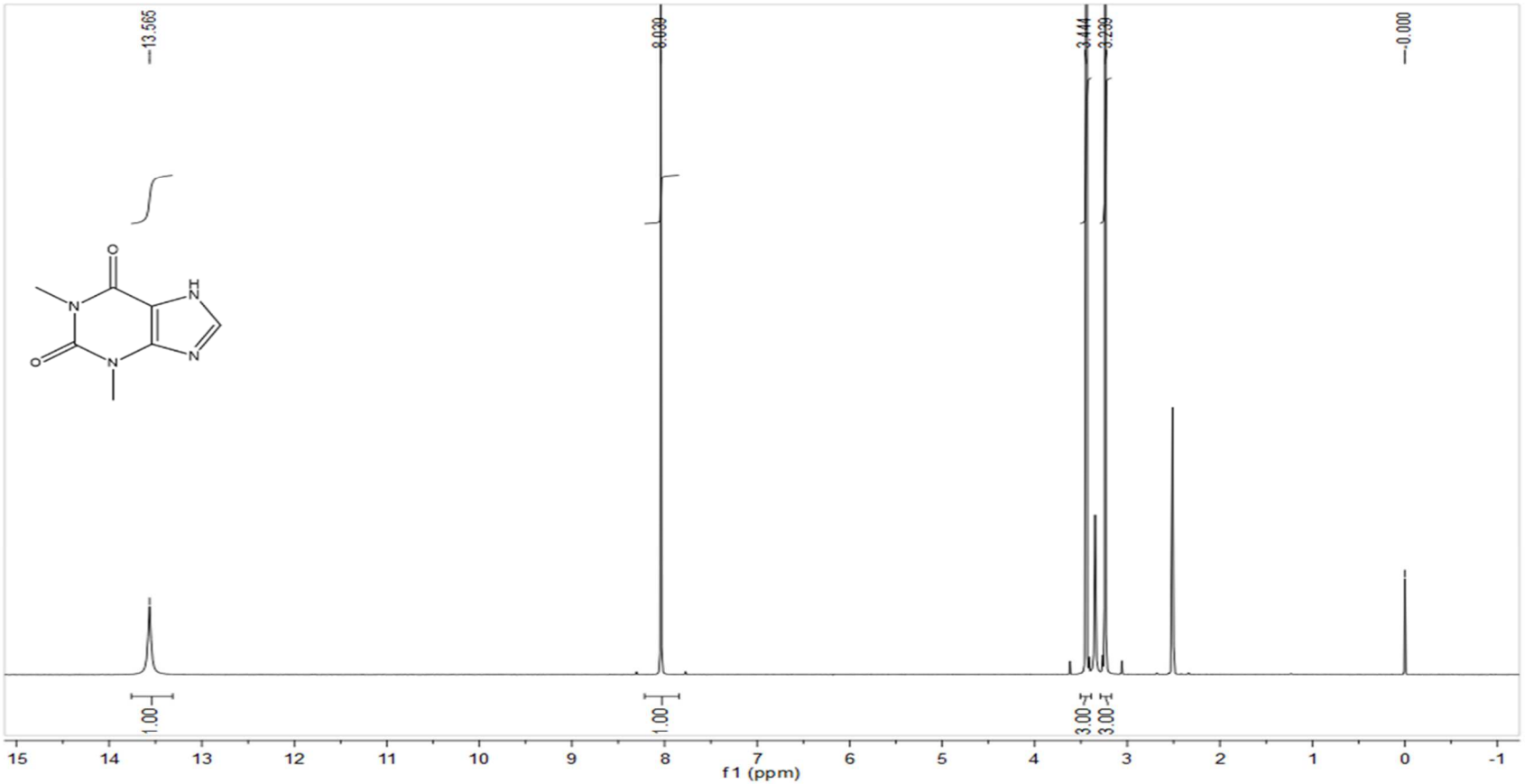

^{1}H NMR (400 MHz, DMSO) δ 13.56 (s, 1H), 8.04 (s, 1H), 3.44 (s, 3H), 3.24 (s, 3H).

SFig. 6. The ^{1}H-NMR for reference standards. (D) M3;

E

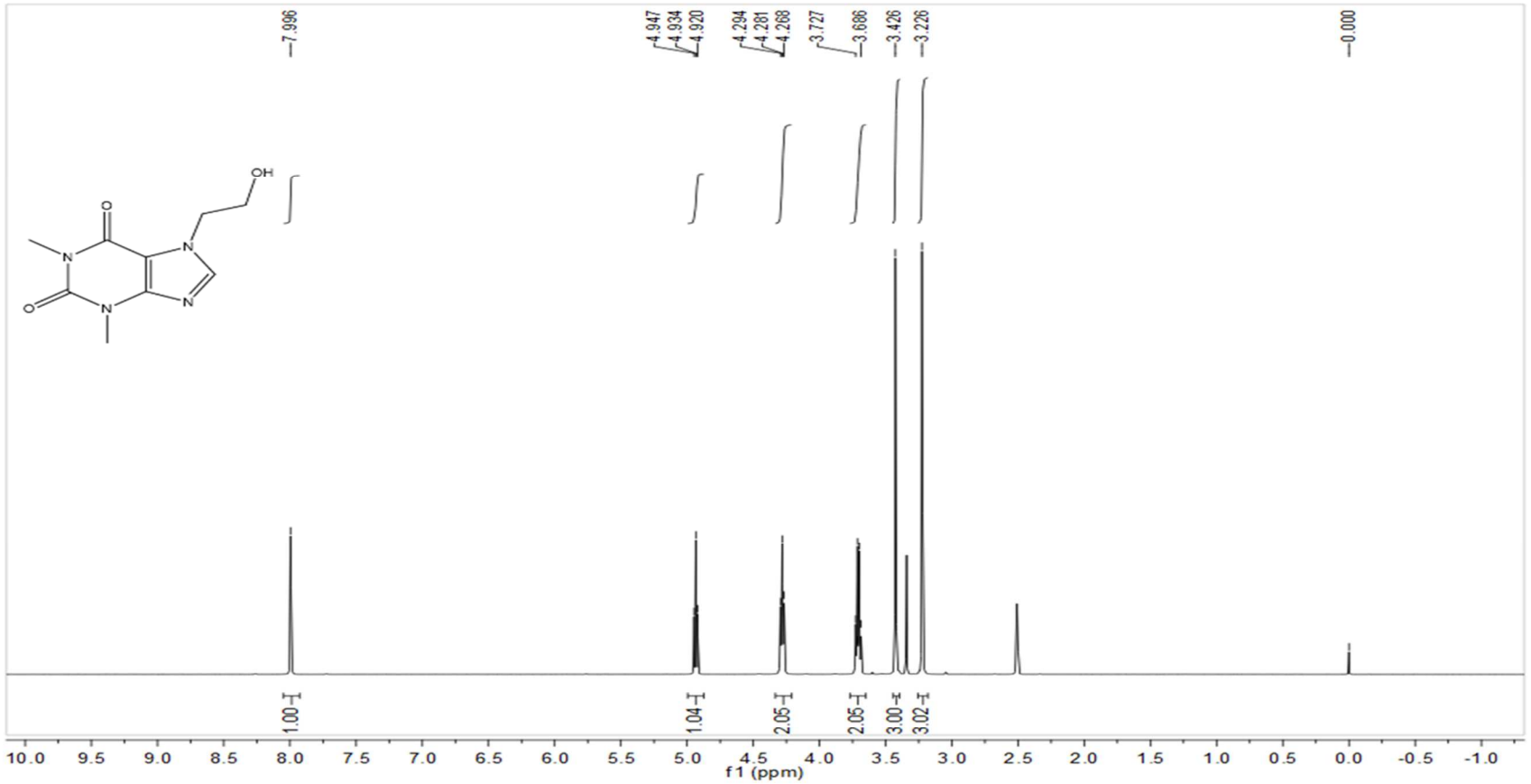

^{1}H NMR (400 MHz, DMSO) δ 8.00 (s, 1H), 4.93 (t, J = 5.4 Hz, 1H), 4.28 (t, J = 5.3 Hz, 2H), 3.71 (m, 2H), 3.43 (s, 3H), 3.23 (s, 3H).

SFig. 6. The ^{1}H-NMR for reference standards. (E) M4;

F

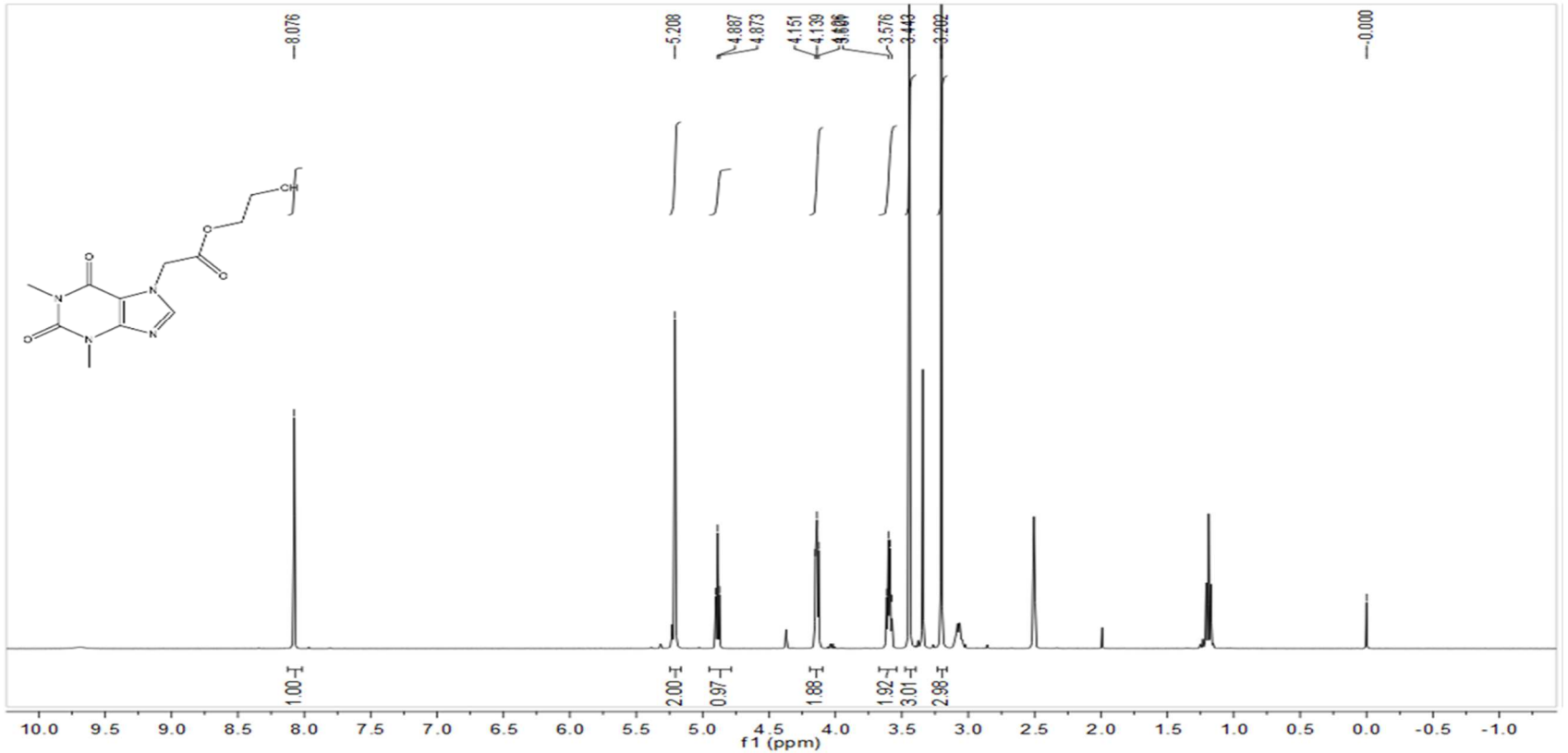

^{1}H NMR (400 MHz, DMSO) δ 8.08 (s, 1H), 5.21 (s, 2H), 4.89 (t, J = 5.5 Hz, 1H), 4.14 (m, 2H), 3.60 (dd, J = 10.2, 5.4 Hz, 2H), 3.44 (s, 3H), 3.20 (s, 3H).

SFig. 6. The ^{1}H-NMR for reference standards. (F) M5.

A

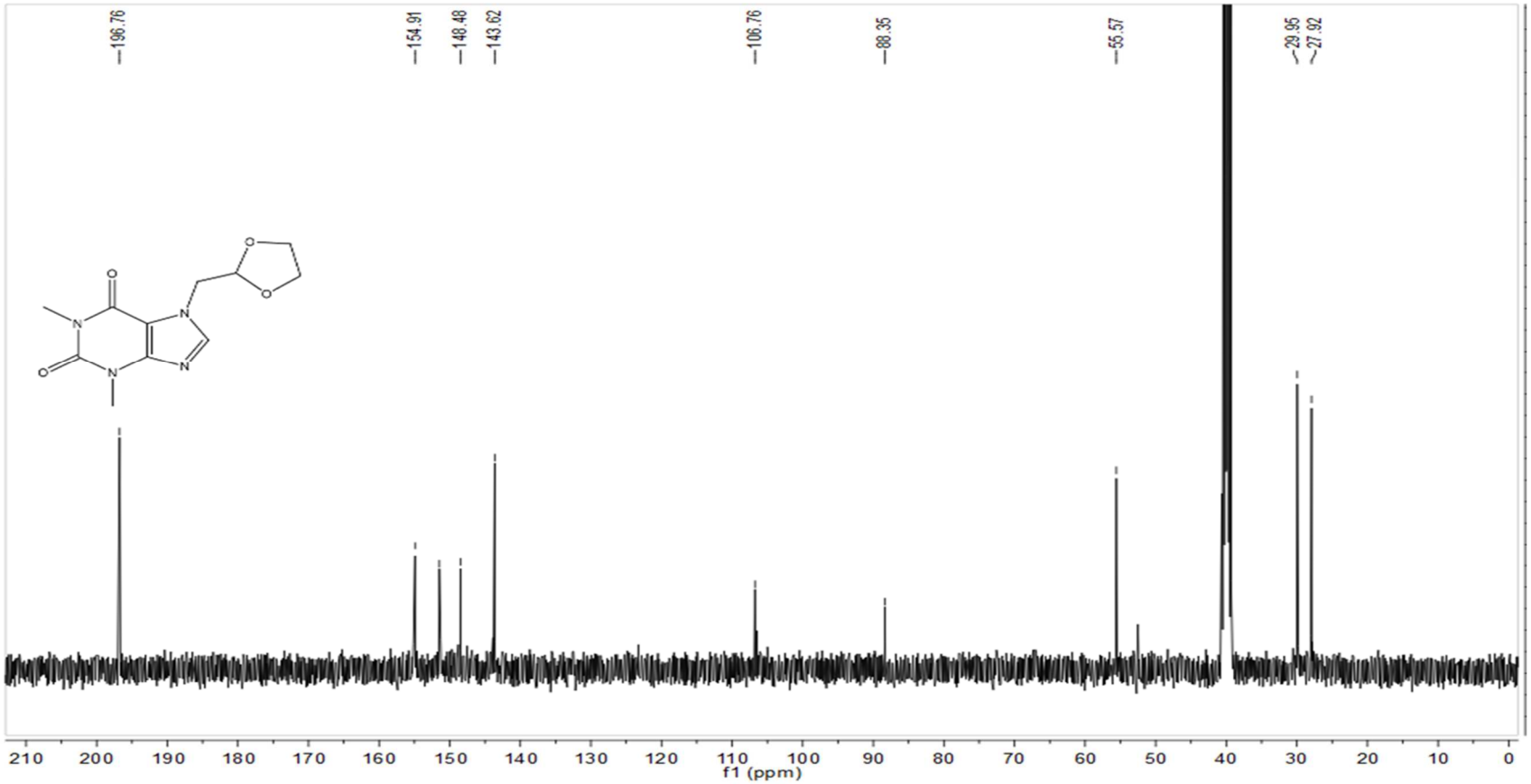

^{13}C NMR (101 MHz, DMSO) δ 196.76, 154.91, 151.47, 148.48, 143.62, 106.76, 88.35, 55.57, 29.95, 27.92.

SFig. 7. The ^{13}C-NMR for reference standards. (A) DOXO;

B

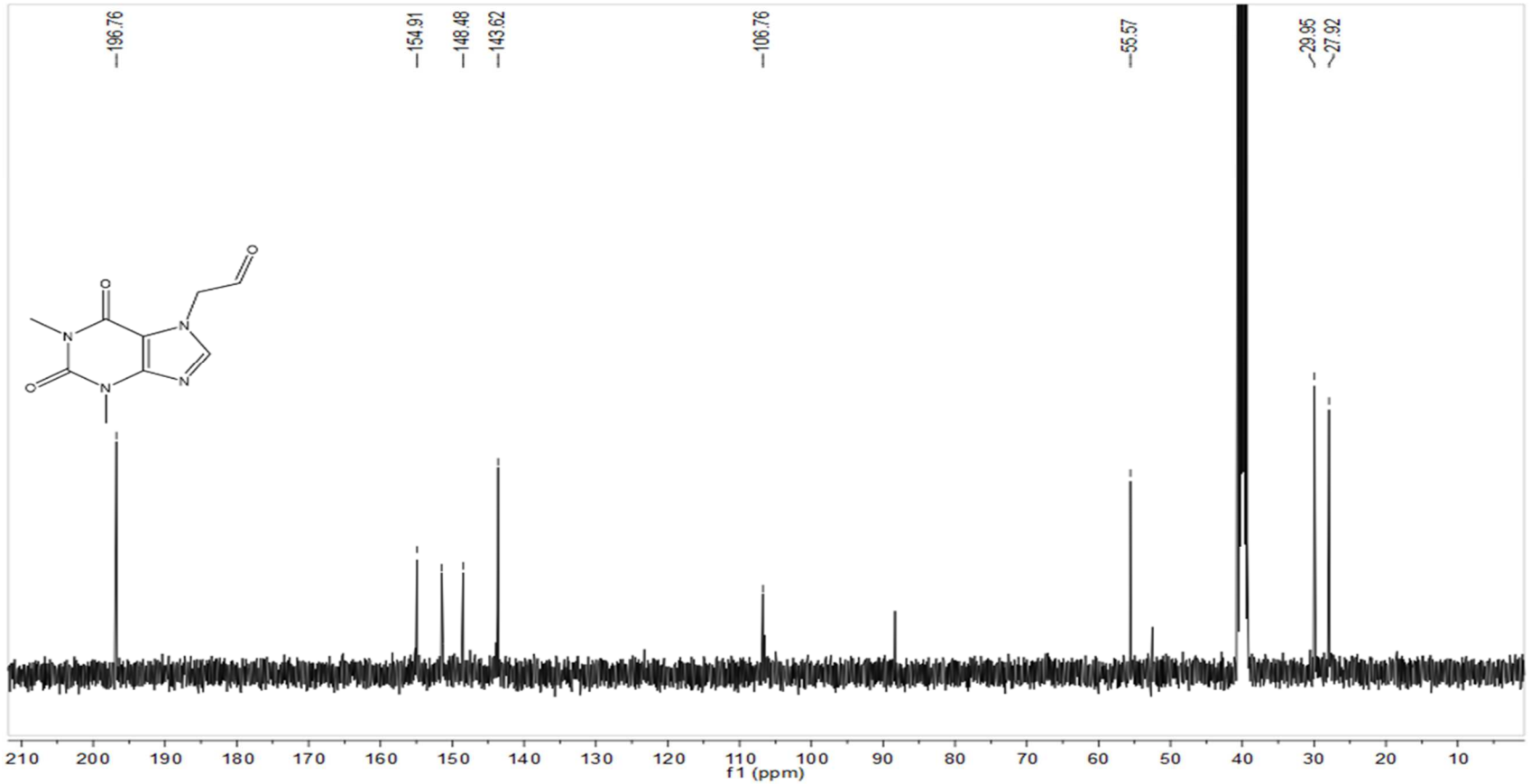

^{13}C NMR (101 MHz, DMSO) δ 196.76, 154.91, 151.47, 148.48, 143.62, 106.76, 55.57, 29.95, 27.92.

SFig. 7. The ^{13}C-NMR for reference standards. (B) M1;

C

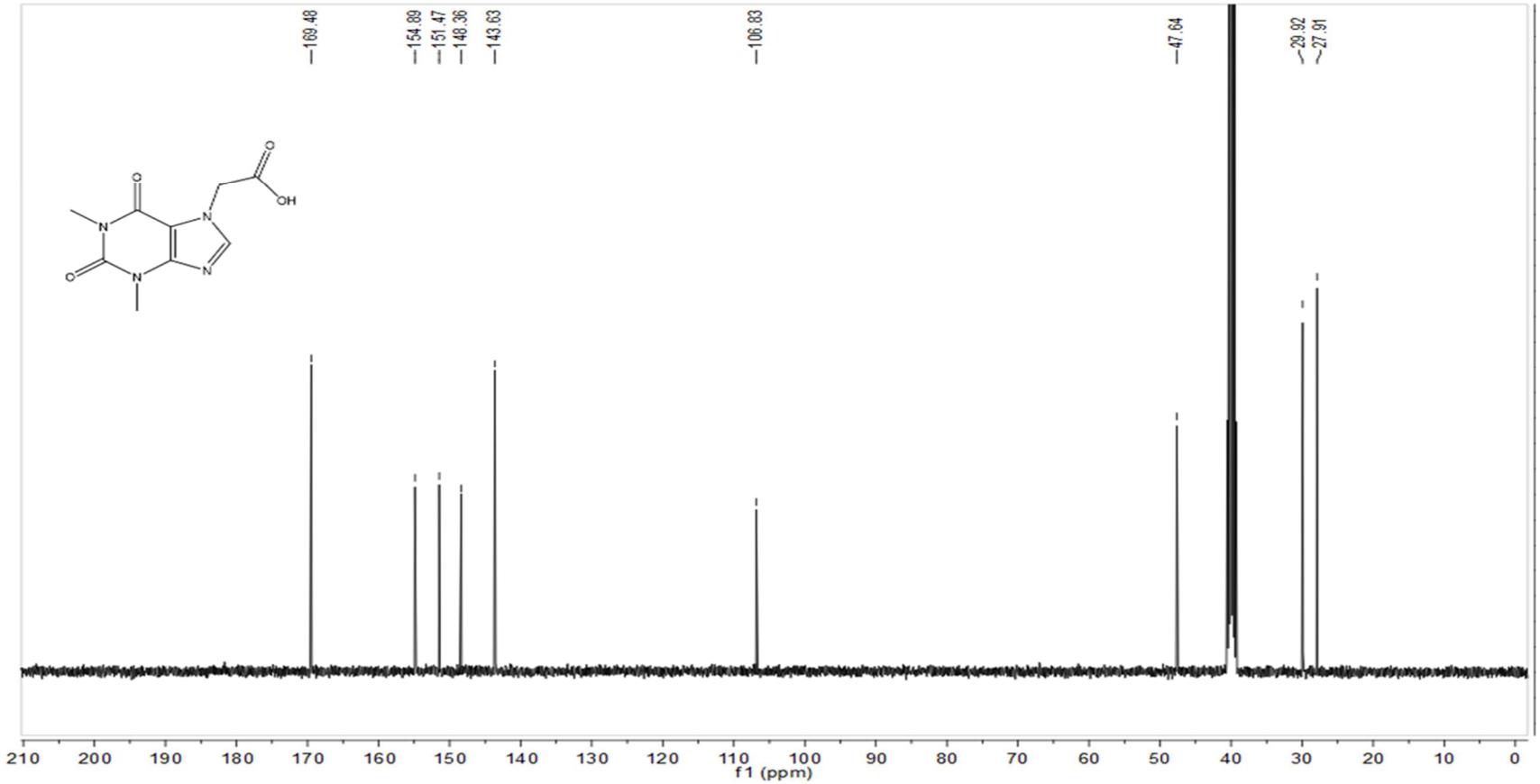

^{13}C NMR (101 MHz, DMSO) δ 169.48, 154.89, 151.47, 148.36, 143.63, 106.83, 47.64, 29.92, 27.91.

SFig. 7. The ^{13}C-NMR for reference standards. (C) M2;

D

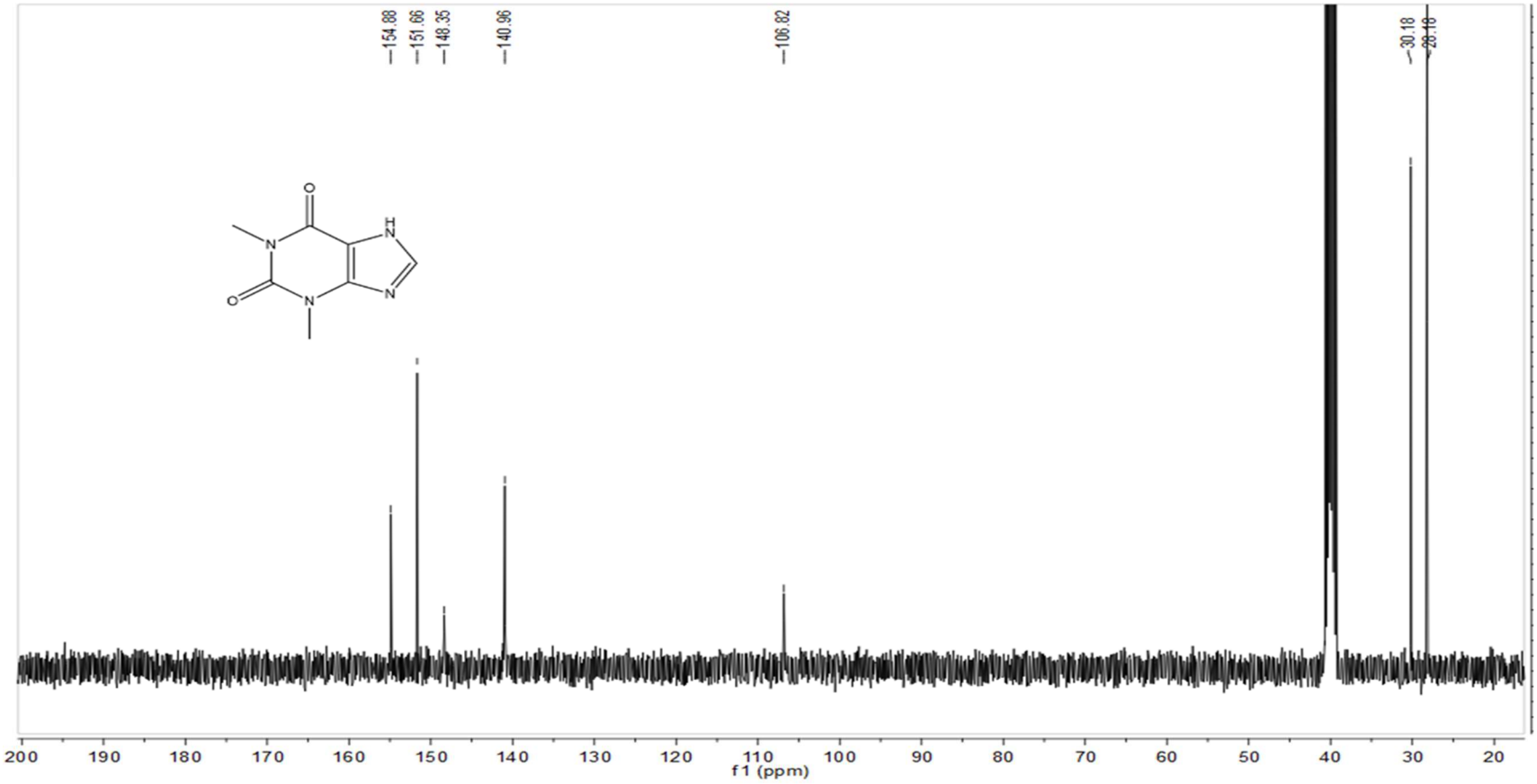

^{13}C NMR (101 MHz, DMSO) δ 154.88, 151.66, 148.35, 140.96, 106.82, 30.18, 28.18.

SFig. 7. The ^{13}C-NMR for reference standards. (D) M3;

E

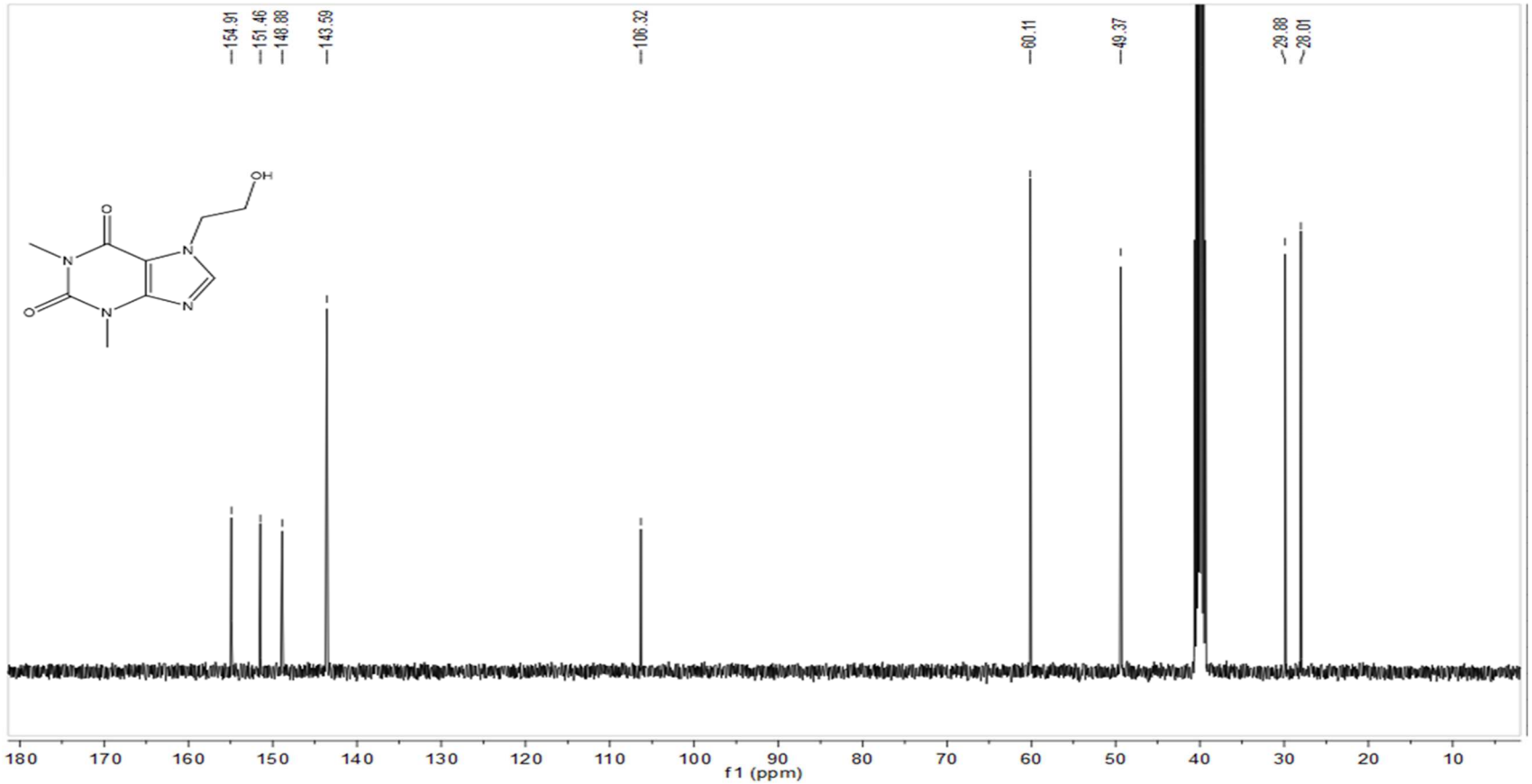

^{13}C NMR (101 MHz, DMSO) δ 154.91, 151.46, 148.88, 143.59, 106.32, 60.11, 49.37, 29.88, 28.01.

SFig. 7. The ^{13}C-NMR for reference standards. (E) M4;

F

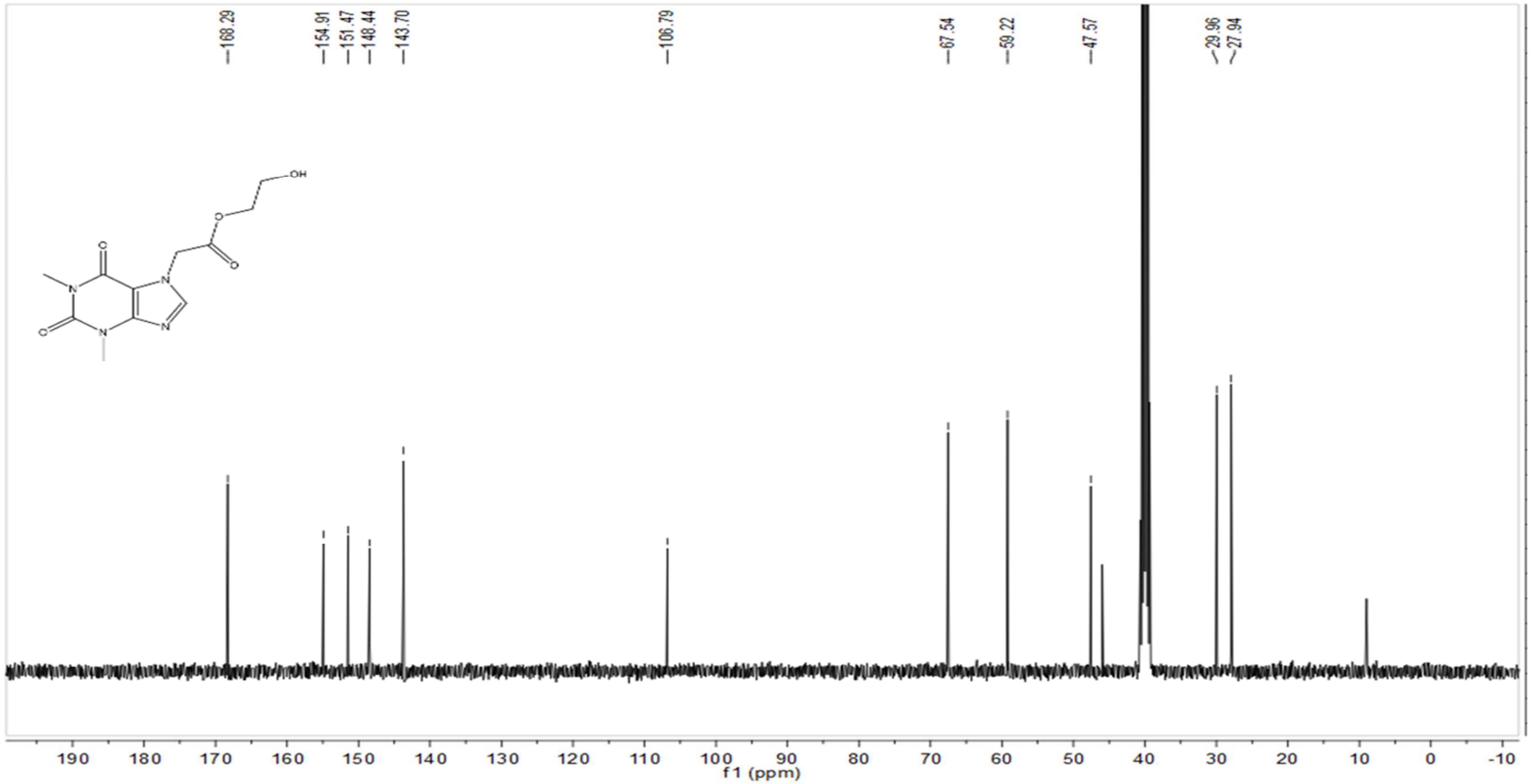

^{13}C NMR (101 MHz, DMSO) δ 168.29, 154.91, 151.47, 148.44, 143.70, 106.79, 67.54, 59.22, 47.57, 29.96, 27.94.

SFig. 7. The ^{13}C-NMR for reference standards. (F) M5.

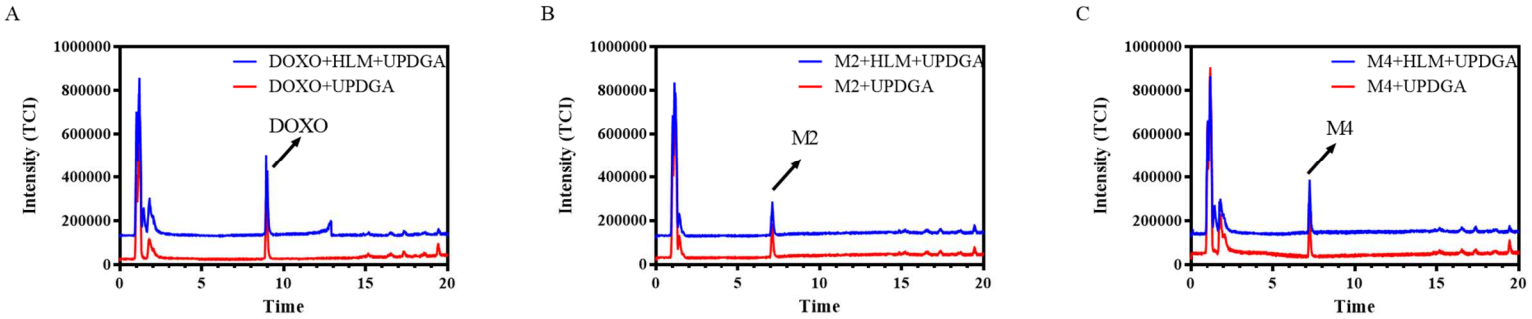

SFig. 8. TIC chromatogram of different substrates in phase II metabolism incubation system in the presences or absence of HLM determined by LC-Triple TOF. (A) DOXO; (B) M2; (C) M4.

Supplemental Table

STable 1. The ion transitions monitored for DOXO and metabolites.

analyte	Q1 Mass (Da)	Q3 Mass (Da)	Dwell (msec)
DOXO	267.1	181.1	60
M1	241.1	181.1	60
M2	239.1	181.1	60
M4	225.1	181.1	60
M5	283.1	239.1	60
M8	253.1	167.1	60
M9	265.1	181.1	60

STable 2. Metabolites of DOXO detected by LC-Triple TOF in HLM.

	Rt				Error						
	min	Measured	Ion	Formula	ppm	Product ions (m/z)	HLM	MLM	RaLM	RLM	CyLM
M0	6.68	267.1085	$[M+H]^+$	$C_{11}H_{14}N_4O_4$	-1.0	223.0814, 210.0867, 181.0712, 166.0602, 138.0654, 124.0494					
M1	5.10	241.0935	$[M+H_2O+H]^+$	$C_9H_{10}N_4O_3$	1.5	223.0828, 195.0875, 181.0720, 166.0611, 138.0660, 124.0499	+++	+++	+++	+++	+++
M2	4.65	239.0772	$[M+H]^+$	$C_9H_{10}N_4O_4$	-1.2	221.0653, 181.0708, 138.0640, 124.0495	+	++	+	+	+
M3	4.67	181.0714	$[M+H]^+$	$C_7H_8N_4O_2$	-3.3	124.0502, 139.9619	+	+	+	+	+
M4	5.24	225.0969	$[M+H]^+$	$C_9H_{12}N_4O_3$	-5.9	207.0872, 181.0713, 124.0490	+	+++	+++	+	++
M5	5.58	283.1033	$[M+H]^+$	$C_{11}H_{14}N_4O_5$	-1.4	265.0192, 239.0712, 181.0711, 124.0502	+	+++	++	+++	++
M6	5.84	283.1034	$[M+H]^+$	$C_{11}H_{14}N_4O_5$	-1.1	267.0142, 239.0779, 197.0662	+	+	+	+	+
M7	5.18	253.0928	$[M+H]^+$	$C_{10}H_{12}N_4O_4$	-1.3	167.0558	+	+	+	+	+
M8	5.72	253.0920	$[M+H]^+$	$C_{10}H_{12}N_4O_4$	-4.9	167.0558	+	+	+	+	+
M9	6.36	265.0923	$[M+H]^+$	$C_{11}H_{12}N_4O_4$	-3.1	181.0710	+	+	+	+	+

STable. 3. The HPLC condition for purity test.

column	VP-ODS 3.0×100 mm 4.6 μm
mobile phase	A: 0.2% formic acid; B acetonitrile 0~2 min: 2%B 2~28 min: 2%B~90%B 28~30 min: 90%B 30.1min: 2%B
Flow:	0.8 mL/min
Temperature:	30℃
Detector:	UV@273
Injection volume:	10 μL

STable. 4. Representative calibration curves for DOXO, M1, M2, M4, and M5.

analyte	curve	r^2
DOXO	y=4034.84212 x + 117.49016	0.9936
M1	y=1260.46153 x + 174.46048	0.9952
M2	y=1205.52800 x + 97.24184	0.9969
M4	y=2683.56612 x + 654.08111	0.9943
M5	y=1803.35266 x + 1165.32597	0.9917